



University of  
Zurich<sup>UZH</sup>

---

---

neuro2voc: Decoding Vocalizations from Neural Activity

---

---

MASTER'S THESIS

PRESENTED TO THE FACULTY OF ARTS AND SOCIAL SCIENCES OF  
THE UNIVERSITY OF ZURICH FOR THE DEGREE OF

MASTER OF ARTS

AUTHOR  
FEI GAO

PRINCIPAL INVESTIGATORS  
PROF. DR. NATHALIE GIROUD  
PROF. DR. RICHARD HAHNLOSER

SUPERVISORS  
MARIS BASHA  
DR. CORINNA LORENZ  
DR. REMO NITSCHKE

DATE OF SUBMISSION: NOVEMBER 30, 2024

# Abstract

Accurate decoding of neural spike trains and relating them to motor output is a challenging task due to the inherent sparsity and length in neural spikes and the complexity of brain circuits. This master project investigates experimental methods for decoding zebra finch motor outputs (in both discrete syllables and continuous spectrograms), from invasive neural recordings obtained from Neuropixels.

There are three major achievements: (1) XGBoost with SHAP analysis trained on spike rates revealed neuronal interaction patterns crucial for syllable classification. (2) Novel method (tokenizing neural data with GPT2) and architecture (Mamba2) demonstrated potential for decoding of syllables using spikes. (3) A combined contrastive learning-VAE framework successfully generated spectrograms from binned neural data.

This work establishes a promising foundation for neural decoding of complex motor outputs and offers several novel methodological approaches for processing sparse neural data.

# Acknowledgment

First and foremost, I would like to express my sincere gratitude to Prof. Dr. Richard Hahnloser for providing me with the opportunity to undertake this project and providing valuable feedback. I am equally grateful to Prof. Dr. Nathalie Giroud for her continued support throughout my academic journey.

I would like to extend my gratitude to my supervisors: Corinna, Maris, and Remo. I am deeply grateful to Corinna for her excellent data, patient guidance and detailed feedbacks on the intricate details of the project. I thank Maris for his ideas and consistent input on potential directions, as well as valuable feedbacks on presentation slides. His contribution of the NeuralEnCodec repository is the foundation for my subsequent EnCodec implementations. I am grateful to Remo for his thoughtful feedback, help and guidance on the tools, catch-ups, and insights into model interpretability. I would like to thank all three of my supervisors again for their help and feedback. Their collective mentorship have been invaluable to the completion of this thesis.

I would also like to thank Aidan, Jacob, as well as all members in the Birdsong and Natural Language Group for their feedback and patience during my presentations.

My sincere thanks to all amazing administrative team members at the Institute of Computational Linguistics and Institute of Neuroinformatics for their invaluable administrative support for this thesis.

Finally, I want to express my heartfelt gratitude to Zhugu, my friends, and my family for their unwavering support. This thesis would not have been possible without their unconditional support.

# Contents

<b>Acknowledgment</b>	<b>ii</b>
<b>1 Introduction</b>	<b>1</b>
1.1 Motivation . . . . .	1
1.2 Research Question . . . . .	2
1.3 Methodological Framework . . . . .	2
1.4 Thesis Structure . . . . .	3
<b>2 Related Work</b>	<b>4</b>
2.1 Representation Learning Approaches . . . . .	4
2.2 Deep Learning Approaches . . . . .	6
<b>3 Dataset</b>	<b>8</b>
3.1 Data Overview . . . . .	8
3.2 Neural Data . . . . .	8
3.3 Vocal Data . . . . .	10
<b>4 Methodology</b>	<b>12</b>
4.1 Mamba . . . . .	12

---

4.2	SHapley Additive exPlanations Interaction Values . . . . .	14
4.3	Support Vector Machine . . . . .	14
4.4	TF-IDF . . . . .	15
4.5	Transformers . . . . .	16
4.6	Variational Auto-Encoders . . . . .	18
<b>5</b>	<b>Experiment 1: Machine Learning Benchmarks</b>	<b>21</b>
5.1	Methods . . . . .	21
5.2	Results . . . . .	23
5.3	Discussion . . . . .	33
<b>6</b>	<b>Experiment 2: Token-based Deep Learning Methods</b>	<b>35</b>
6.1	Methods . . . . .	35
6.2	Results . . . . .	37
6.3	Discussion . . . . .	39
<b>7</b>	<b>Experiment 3: Temporal Deep Learning Methods</b>	<b>40</b>
7.1	Methods . . . . .	40
7.2	Results . . . . .	41
7.3	Discussion . . . . .	44
<b>8</b>	<b>Experiment 4: CEBRA Latent Embeddings</b>	<b>46</b>
8.1	Methods . . . . .	46
8.2	Results . . . . .	48
8.3	Discussion . . . . .	52
<b>9</b>	<b>Experiment 5: VAE Latent Representations</b>	<b>53</b>

---

9.1	Methods . . . . .	53
9.2	Data Preparation . . . . .	54
9.3	Models and Evaluation . . . . .	56
9.4	Visualization Results . . . . .	57
9.5	Latent Representation Evaluations . . . . .	67
9.6	Canonical Component Analysis . . . . .	69
9.7	Discussion . . . . .	70
<b>10</b>	<b>Conclusion</b>	<b>71</b>
10.1	Achievements . . . . .	71
10.2	Limitations . . . . .	72
10.3	Future Direction . . . . .	73
	<b>References</b>	<b>74</b>
<b>A</b>	<b>Appendix</b>	<b>81</b>
A.1	Neuron Depths . . . . .	81
A.2	Neural Information Integration . . . . .	82
A.3	CEBRA Results . . . . .	83
A.4	VAE Results . . . . .	85

# Chapter 1

## Introduction

Recent advances in neural recording technologies and speech analysis methods have created new possibilities to address challenges during analyzing the relationship between neural activity and behaviours. The challenges stem from the complex nature of spike trains – sparse, long, and high dimensional – as well as the need to align them with complex behavioural labels or external stimuli. For this project, we worked on bird vocalizations and the corresponding neural signals. We benefited from Neuropixels (Jun et al., 2017), which allows for extremely high temporal and spatial resolution recording of neural spikes in animals, and from methods that enable effective extraction of syllable clusters from the bird vocalizations (Lorenz et al., 2022). With these advances, we attempted to address some challenges in correlating spike train data with vocalization.

### 1.1 Motivation

This project is motivated by recent technological advances in Machine Learning (ML). First, Natural Language Processing (NLP) techniques have demonstrated remarkable success in text-processing. Transformer models excel at handling sentences, and have been adapted to handle sparse and long sequential data – a characteristics shared with neural spike data. Second, recent Mamba architectures (Gu and Dao, 2023; Dao and Gu, 2024) efficiently process long sequences without the quadratic bottleneck which transformers have. These advances offer a perspective to address some key challenges in neural data analysis: the inherent sparsity of spike data and the need for long-range

dependencies.

In addition, with emergent representation learning techniques, such as Variational Auto-Encoder (VAE) architecture and contrastive learning method, we would like to investigate correlations between neural data and behavioural data at a finer temporal scale.

## 1.2 Research Question

Our project aimed to address three questions:

1. Can we validate spike based classification method for syllables of Zebra Finch?
2. How well can natural language processing methods and different deep learning architectures handle long, sparse, and high-dimensional spike data?
3. Can we effectively map spike data to latent spaces for classification and reconstruction?

## 1.3 Methodological Framework

To answer these questions, we developed a three-part methodological framework:

### 1.3.1 Baseline Validation

We first established performance benchmarks for syllable-based classification through classical ML methods: Support Vector Machine (SVM), Random Forest (RF), and XG-Boost. In addition, we used SHAP values to analyze the interaction between neurons.

### 1.3.2 Deep Learning Methods

Then, we explored various neural data analysis methods. We used a tokenization method to analyze the data with GPT-2. We implemented several models, including Mamba-2 and EEGNet (Lawhern et al., 2016), to deal with long range temporal dependencies over tokenized and time series data.

### 1.3.3 Representational Learning

We used CEBRA methods and VAE architecture to obtain interpretable latent representations from our neural data. We created a joint VAE with contrastive learning methods to map neural data into vocalizations. We evaluated all obtained representations on syllable classification tasks.

The code is publicly available at [https://github.com/askrbayern/neuro2voc\\_thesis](https://github.com/askrbayern/neuro2voc_thesis).

## 1.4 Thesis Structure

The remainder of this thesis is divided into the following chapters:

- Chapter 2: Related Work
- Chapter 3: Dataset
- Chapter 4: Methodology
- Chapter 5–9: Experiments  
Each chapter describes one key experiment, including:
  - Experiment 1 Machine Learning Benchmarks
  - Experiment 2 Token-based Deep Learning Methods
  - Experiment 3 Temporal Deep Learning Methods
  - Experiment 4 CEBRA Latent Embeddings
  - Experiment 5 VAE Latent Representations
- Chapter 10: Conclusion

## Chapter 2

# Related Work

Research has shown that juvenile zebra finch birds learn to sing through a complex sensorimotor process (Doupe and Kuhl, 1999). The birds progress from simple and highly variable sub-songs to fixed and distinct songs during learning. A direct motor pathway connects HVC to nucleus RA and controls the production of the song (Gale and Perkel, 2010). HVC is also connected to RA through a second pathway, the anterior forebrain pathway (AFP). AFP controls the song variability, song learning and plasticity (Doupe et al., 2005). In this pathway, HVC is connected to RA through area X, DLM, and LMAN in sequence. In this pathway, LMAN projects back to the area X in this circuit, thus forming a recursive loop. Research has shown that lesions from the LMAN area in this sensorimotor process stop adult birds from adapting spectral features of their song by operant conditioning (Andalman and Fee, 2009; Bottjer et al., 1984).

### 2.1 Representation Learning Approaches

Previous work by Singh Alvarado et al. (2021) investigated the variability of performance in male zebra finch birds in two conditions: solo practice (undirected singing) and performing (directed singing). They developed finchVAE, a Variational Auto-Encoder (VAE), to extract the latent representations of both neural and vocal data, and analyze the relationship between the latent embeddings.

While only using undirected song data, we extended their work in two ways. First, with annotated syllables from (Lorenz et al., 2022), we could focus on a finer scale of syllables

instead of motifs, which is composed of several different syllables. Second, we adapted the original model on another type of neural recordings. The main challenge comes from the fact that the original paper used Calcium imaging as neural recordings, while our neural data was a time series collected from Neuropixels 1.0 (Jun et al., 2017) and then spike-sorted with Kilosort (Pachitariu et al., 2016). VAEs were originally designed to deal with image data (Kingma and Welling, 2013, 2019), which is well-suited for the Calcium imaging data. For our time series data, we were particularly inspired by EnCodec from Défossez et al. (2022b), a VAE structure for high-fidelity neural audio compression that utilizes quantization techniques and codebooks. The concept of codebooks originated from Vector Quantized VAE (VQ-VAE) proposed by van den Oord et al. (2017) and was later put into work by Zeghidour et al. (2021). In VQ-VAE, the codebook is used to map continuous representations into discrete codes. We implemented EnCodec and devised different types of VAEs based on finchVAE to deal with spike data.

Researchers have also explored contrastive learning methods to decode neural data (Schneider et al., 2023; Défossez et al., 2022a). Schneider et al. (2023) proposed the CEBRA method which processes time-series neural recordings, and generates latent embeddings for each time point. In the paper, the latent embeddings were used to decode neural responses in the visual cortex of mice that were watching a repeating video, and 95% of the frames were correctly identified in the test dataset. We aim to use this method, and use different syllables to supervise the training. For human speech, Défossez et al. (2022a) proposed brainmagick, a contrastive learning based method to decode the speech heard from non-invasive brain recordings, such as Electroencephalogram (EEG) or Magnetoencephalography (MEG). They successfully aligned the neural responses with acoustic stimuli. For neural data, the best result came from the MEG data due to the high spatial accuracy of MEG. They first generated latent embeddings of non-invasive recordings through a Convolutional Neural Network. The speech embeddings were either from Mel Spectrogram, or taken from pre-trained models like wav2vec 2.0 (Baeovski et al., 2020). The embeddings of two modalities were compared using Contrastive Language-Image Pre-Training (CLIP) loss. During our reproduction of brainmagick on the data of Gwilliams et al. (2022), the model correctly identified the word heard with 40 % accuracy from MEG data and had a Top 10 accuracy of 69 %.

In conclusion, the above representation learning methods show great potential for neural decoding. VAE excels at data compression and is generative in nature, while contrastive learning methods like CEBRA offer great decoding capability as well as fine temporal resolution. As a result, we combined VAE with contrastive learning in the last task.

There are several representation learning methods for neural data unexplored in this project: GP-VAE (Gondur et al., 2023), MARBLE (Gosztolai et al., 2023), pi-VAE (Zhou and Wei, 2020), TiDeVAE (Huang et al., 2024), etc.

## 2.2 Deep Learning Approaches

With recent advances in Natural Language Processing (NLP) and Machine Learning (ML) architectures, we aimed to use these new tools to deal with the spike train data. Spike train data is composed of spikes, or action potentials, which are discrete electrical signals generated by neurons as a result of underlying cellular and molecular activities. Spike train data is in nature very sparse. In Natural Language Processing (NLP), sparsity can be used to refer to either data sparsity or model sparsity. Data sparsity refers to large embedding sizes where only a few dimensions have significant values (Farina et al., 2024). The most typical case would be One-Hot-Encodings, where each word is represented by a column vector of the length of the vocabulary, and all the positions are zero, except that the position for the current word has a one. Model sparsity refers to a neural network with a lot of empty weights, which could either increase the performance (Child et al., 2019) or reduce performance by missing out important information (Farina et al., 2024).

The sparsity in spike train data is similar to data sparsity described above. One drawback brought up by sparse spikes is that the activity patterns are encoded in a long ‘One-Hot-Encodings’ where only a small part is meaningful. Transformer is not the best architecture to deal with long sequences, but there has been some work on this direction (Li et al., 2023). In addition to this, transformers are resource-demanding. The computational complexity is quadratic to the sentence length, coming from the dot product calculation of the attention.

Nevertheless, there are a few promising work done in this direction. Azabou et al. (2023) proposed a transformer-based framework Pre-training On manY neurOns (POYO). POYO treats the neural spikes as discrete tokens, and pretrains the model on large-scale recordings to improve the performance on decoding tasks. In this project, we also explored the tokenization method.

Although transformers can handle the sparse data to some extent, they are not the best models to use. With the quadratic bottleneck of transformers, it consumes a lot of

time and computational resources to train and inference. Gu and Dao (2023) proposed Mamba, a Structured State-Space Model, that only has linear complexity. Mamba is specialized at dealing with long sequential data with minimum inference time and resource consumption. Dao and Gu (2024) proposed Mamba-2, a Structured State-Space Duality, which is more efficient than Mamba in training time. With Mamba models, analyzing sparse spike data by addressing data length seems to be more optimistic.

There are a few other methods. Binning is the most commonly used method to resolve this sparsity (Labach et al., 2023). During binning, finer temporal information is lost. (Tipirneni and Reddy, 2021) works on sparse and irregularly sampled data, where they used continuous value embeddings (CVE) to deal with such data. The CVE maps continuous values to high-dimensional spaces using a neural network.

These works show various approaches to process neural data, and each approach offers unique advantage. In our project, we aimed to address the data sparsity issue. Our neural recordings were collected from Neuropixels 1.0 and spike sorted with Kilosort, which produces precise but sparse data. We explored NLP methods and several time series models including Mamba. We also investigated the potential of supervised representation learning methods, and use different VAEs to reconstruct our data.

# Chapter 3

## Dataset

### 3.1 Data Overview

The project used neural and vocal data that were previously collected through three recording sessions from the same bird. During each session, neural and vocal data were recorded simultaneously, thus their start points were the same. Table 3.1 shows the length of recorded vocal and neural data. Extra vocal recordings were removed from the end in this project.

Recording Session	Neural Data Length	Vocal Data Length
Session 0	53.29 min	53.29 min
Session 1	89.91 min	90.06 min
Session 2	70.37 min	77.90 min

Table 3.1: Duration of recordings across different sessions

### 3.2 Neural Data

The preprocessed neural data consists of an array of spike times and an array of spike cluster indices. The data was provided at a sampling rate of 20 kHz. The raw data was collected with Neuropixels 1.0 (Jun et al., 2017) and the preprocessed spike data was obtained through spike-sorting with Kilosort (Pachitariu et al., 2016). All recordings contain only non-directed songs. The data includes additional information: (1) depth,

(2) channel on Neuropixels, (3) firing rate, (4) spike amplitude, and (5) cluster quality.

### 3.2.1 Characteristics of Neurons

Spike-sorting produces clusters of different qualities, which are marked with either good, multi-unit activities (MUA), or noise. In the data used in this project, all neuronal clusters were labeled as either good or MUA. The dataset consists of reliable neural recordings without noisy clusters, making it suitable for further analysis. Figure 3.1 shows the quality of clusters in dark grey and red, with circle diameter indicating the firing rate. LMAN neurons roughly distributed between  $2300\ \mu\text{m}$  and  $3000\ \mu\text{m}$ .

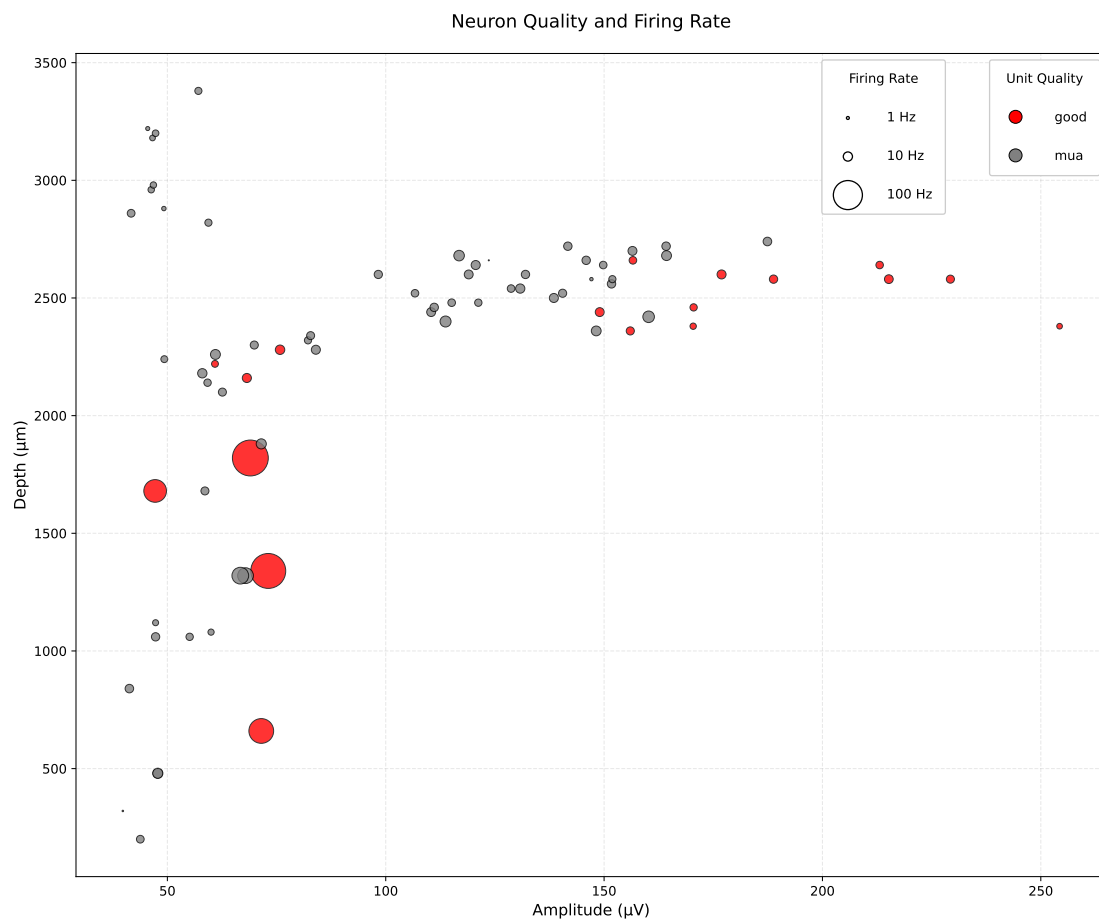


Figure 3.1: Quality of clusters

### 3.3 Vocal Data

The vocal recordings were obtained from recording devices in the lab. The raw data was preprocessed by first downsampling from 20 kHz to 250 Hz, and then applying a STFT with a 16 ms offset (64 samples under 250 Hz). The data used for this project were prepared in spectrograms in 128 frequency bins ranging from [0 Hz, -8000 Hz] in 250 Hz. A separate annotation file provides the onset and duration for each vocalization cluster (referred to as syllable in this paper). Our analysis focused on valid vocalization patterns, labeled 2–8. Other syllables were excluded from this investigation. Syllables 2–8 are shown in Figure 3.2.

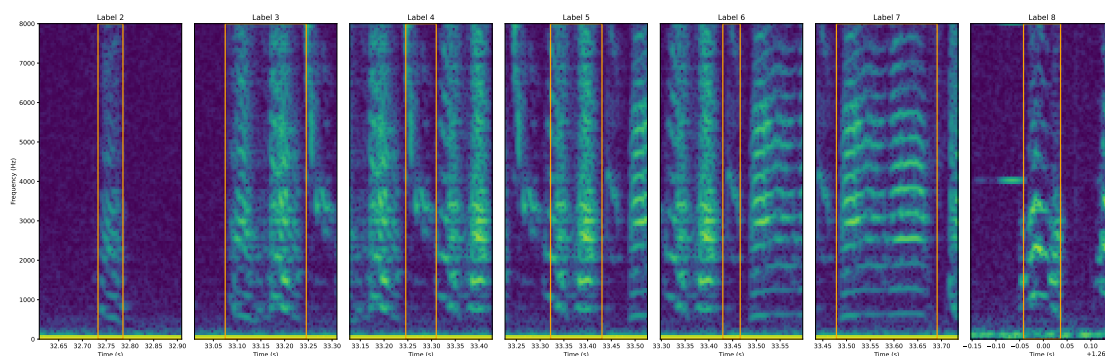
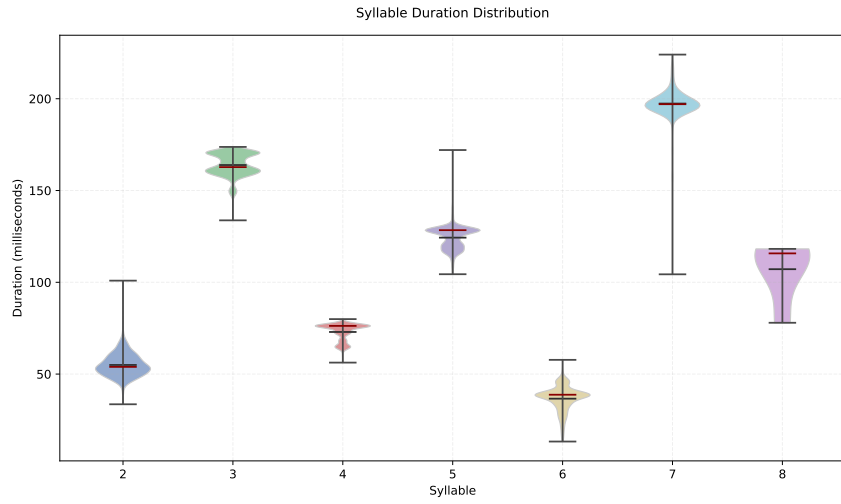


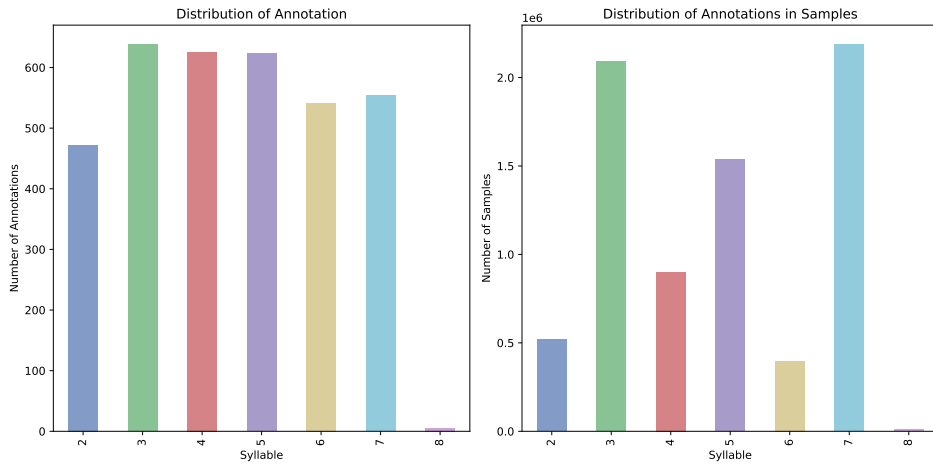
Figure 3.2: Labeled spectrogram for all 7 syllables

#### 3.3.1 Distribution of Syllables

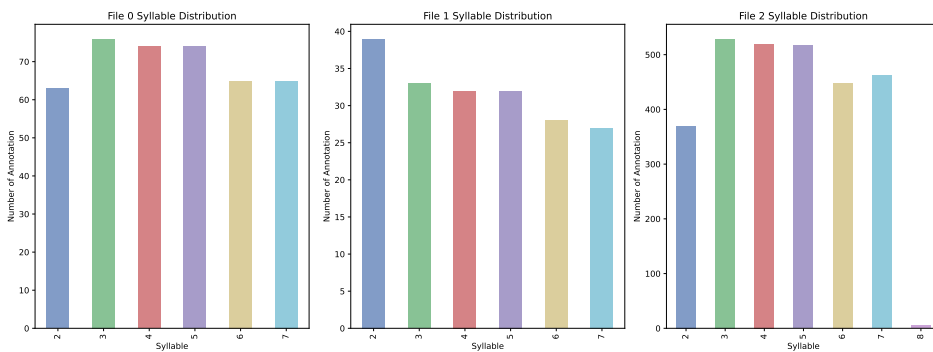
Figure 3.3a shows that there is considerable variation in syllable length. Figure 3.3b shows syllables 2–7 occur at similar frequencies, while syllable 8 occurs rarely. On a sampling rate level, however, Figure 3.3b shows that the data is imbalanced on a sampling time level, where label 3, 5, and 7 together take up 80% of the sampling time data. Figure 3.3c shows that the syllable distributions are similar across sessions.



(a) Distribution of syllable lengths



(b) Total distribution of syllables



(c) Distribution of syllables per session

Figure 3.3: Distribution of annotated syllables

# Chapter 4

## Methodology

### 4.1 Mamba

#### 4.1.1 Selective State Space Model

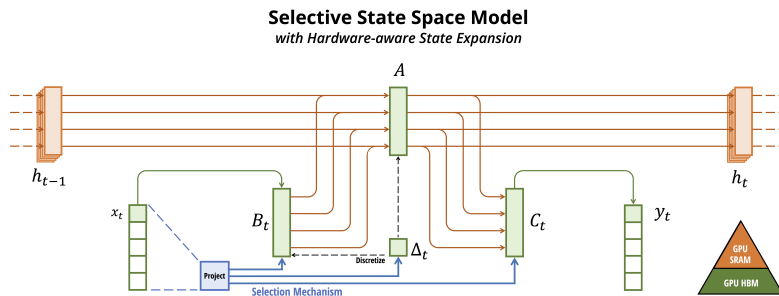


Figure 4.1: Selective State Space Model

$$h_t = g(\mathbf{A}_t h_{t-1} + \mathbf{B}_t x_t)$$

$$y_t = \mathbf{C}_t^T h_t$$

$\mathbf{A}_t \in \mathbb{R}^{N,N}$  : state to state transition matrices

$\mathbf{B}_t \in \mathbb{R}^N$  : input to state transition vector

$\mathbf{C}_t \in \mathbb{R}^N$  : state to output transition vector

$g$  : activation function

A selective state space model (SSM) is defined above, where  $\mathbf{A}$ ,  $\mathbf{B}$ , and  $\mathbf{C}$  are the three parameters of the model. Mamba (Gu and Dao, 2023) uses a structured SSM, which is a selective SSM with  $\mathbf{A}_t$  being a diagonal matrix.

### 4.1.2 State Space Duality

Mamba-2 Dao and Gu (2024) uses the state space duality (SSD) structure. SSD is built on SSM with one specification:

$$\mathbf{A}_t = a_t \mathbf{I}$$

$$a_t \in \mathbb{R} : \text{a learnable scalar}$$

This linear mode is also called the SSM mode, which is excellent at inference time due to its computational efficiency. This scalar-identity structured model can be expanded to a quadratic mode, which enables matrix multiplication and dramatically improves the training process. The quadratic mode above can be viewed as:

$$y = \mathbf{M}x$$

$\mathbf{M}$  is a semi-separable matrix similar to causal attention, where  $\mathbf{M}_{ij} = 0$  for  $i < j$  and otherwise

$$\mathbf{M}_{ij} = \prod_{k=j+1}^i a_k \cdot \mathbf{C}_i^\top \mathbf{B}_j$$

### 4.1.3 Mamba and Mamba-2

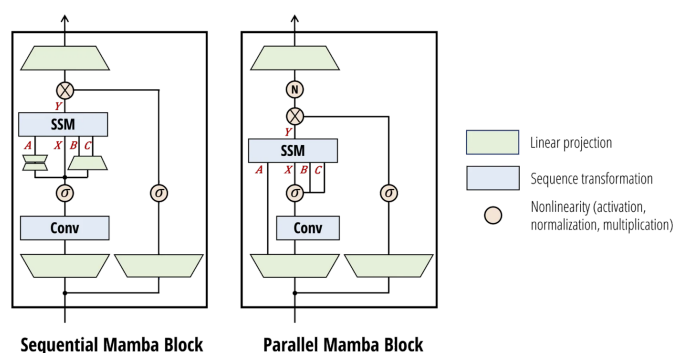


Figure 4.2: Mamba and Mamba-2 structures

Mamba is built upon SSM and uses sequential Mamba block, where **A**, **B**, and **C** are calculated sequentially. Mamba-2 is built upon SSD and uses parallel Mamba block, where **A**, **B**, and **C** are calculated in parallel. Inspired by attention-like architectures, such parallelization accommodates tensor parallelism.

## 4.2 SHapley Additive exPlanations Interaction Values

SHapley Additive exPlanations (SHAP) (Lundberg and Lee, 2017) are used to evaluate the contribution of each feature to model prediction using game theory concepts. SHAP interaction values measure how much the syllable prediction result changes when two neurons' activities are considered together, on top of their individual contributions. A positive pairwise interaction value indicates two neurons work together, and their joint activation provides more information about the syllable than simply adding up their individual contributions. A negative interaction suggests that such joint effect is less than the sum of individual contributions of two neurons, meaning some redundancy in the encoding of information.

## 4.3 Support Vector Machine

Support Vector Machine (SVM) is a supervised machine learning algorithm (Boser et al., 1992) used extensively in this project to establish a benchmark for classification in order to be compared to by all later more complicated methods.

SVM creates an optimal hyperplane by maximizing the margin between classes. The optimal hyperplane is selected by maximizing the margin between classes. A hyperplane can be defined as a homogeneous non-trivial linear equation. In a space of  $R^n$ , a hyperplane has dimensionality of  $R^{n-1}$ . The closest data points to the hyperplane are called the support vectors, and these vectors determine the decision boundary for classification.

Among multiple metrics generated from classification tasks (accuracy, F1, precision, sensitivity, etc.) only overall accuracies are used in this project for simplicity.

$$\min_{w,b,\xi} \frac{1}{2} \|w\|^2 + C \sum_{i=1}^n \xi_i$$

s.t.:

$$y_i (w^T x_i + b) \geq 1 - \xi_i, \quad \xi_i \geq 0, \quad i = 1, 2, \dots, n$$

$w$  : the weight vector

$b$  : the bias

$\xi_i$  : the slack variables that allow for misclassification  
and encode Hinge Loss

$C$  : the regularization parameter

SVMs are conducted with a linear kernel and a Radio Basis Function (RBF) kernel. The linear kernel is defined as

$$K(x, x') = \langle x, x' \rangle$$

The RBF kernel in scikit-learn (Pedregosa et al., 2011) is defined as

$$K(x, x') = \exp(-\gamma \|x - x'\|_2^2)$$

$\gamma$  : the influence range of each training example

$\|x - x'\|_2^2$  : the squared 2-Norm (Euclidean Norm)

For this project, we evaluated both linear and RBF kernels using grid search with scikit-learn. The parameters were: (1)  $C$  parameter: [0.1, 1, 10] (2) gamma parameter (for RBF kernel): [0.01, 0.1, 'scale']

## 4.4 TF-IDF

Term Frequency-Inverse Document Frequency (TF-IDF) is a common feature in the domain of NLP. This feature combines two features: Term Frequency (TF) and Inverse Document Frequency (IDF). TF refers to how often a term appears in a document. IDF refers to how unique this term is across all document. When a term frequently appears in a document but rarely in other documents, the weight of this term would increase. The formula is written as:

$$w_{t,d} = tf_{t,d} \times \log\left(\frac{N}{df_t}\right)$$

$w_{t,d}$  : the weight of term  $t$  in document  $d$

$tf_{t,d}$  : the occurrence frequency of term  $t$  in document  $d$

$N$  : the total number of documents

$df_t$  : the number of documents containing term  $t$

In this project, the same concept has been transferred to neural data. The term refers to the neuron, and the document refers to the data sample with a specific labels. Just like in NLP where the documents can be classified into Law, Medicine, News, etc., the data samples used in this project can be classified into different syllables.

## 4.5 Transformers

Transformers are introduced by Vaswani et al. (2017) and have since established new performance benchmarks in Artificial Intelligence.

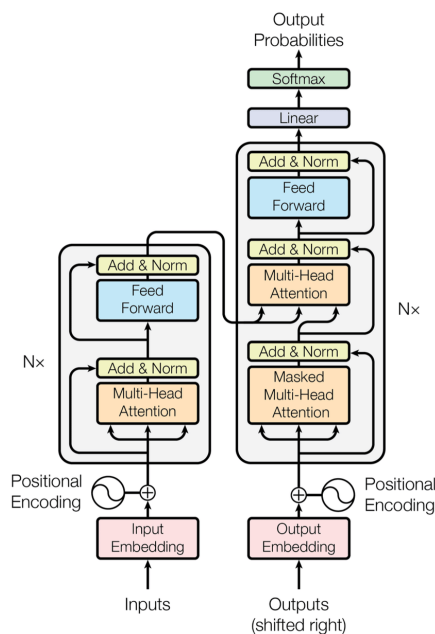


Figure 4.3: Transformers architecture

The Positional Encoding (PE) are added to the input embeddings. Sinusoidal positional

encoding is a basic type of PE introduced in the original paper.

$$PE_{(pos,2i)} = \sin\left(\frac{pos}{10000^{2i/d_{model}}}\right) \quad pos \in [0, n], i \in [0, d_{model}/2]$$

$$PE_{(pos,2i+1)} = \cos\left(\frac{pos}{10000^{2i/d_{model}}}\right) \quad pos \in [0, n], i \in [0, d_{model}/2 - 1]$$

pos : the position in the input sequence

$d_{model}$  : the dimensionality of the embedding vectors

The word embeddings has a size of  $d_{model}$ . The Positional Encoding (PE) matches  $d_{model}$ . In the original transformers (Vaswani et al., 2017),  $d_{model} = 512$ . In OpenAI Generative Pre-trained Transformer (GPT) 2 (Radford et al., 2019) that we used in experiment 2,  $d_{model} = 768$ .

$$\text{score}(x_i, x_j) = \frac{q_i \cdot k_j}{\sqrt{d_k}}$$

$$[\alpha_{ij}] = \text{softmax}(\text{score}(x_i, x_j)) \quad \forall j \leq i$$

$$a_i = \sum_{j \leq i} \alpha_{ij} v_j$$

The calculation for masked attention used in GPT is shown above. The attention weights are calculated by doing pair-wise dot product between key and query, and the scores are divided by  $\sqrt{d_k}$  to reduce the variance from dot products. Then softmax is applied to the scores, and creates attention weights. The attention weights are multiplied by values and produces the attention output. In Multi-Head Attention (MHA), the outputs of individual heads are stacked.

$$x = \text{MHA}(x) + \alpha x, \quad \alpha \in [0, 1]$$

$$\text{LayerNorm}(x) = \gamma \frac{x - \mu}{\sigma} + \beta$$

$\alpha$  : scaling factor for the residual connection

$\mu$  : mean of the input

$\sigma$  : standard deviation of the input

$\gamma$  and  $\beta$  : learnable parameters

The add operation is called the residual connection. It ensures that the transformed output is close to the input shape. The normalization is applied after every layers to control the value ranges. The layer norm is the most popular normalization. In layer normalization, the activations are normalized (demeaned and then divided by the standard deviation) over the feature dimensions ( $d_{\text{model}}$ ) for each example in the batch.

$$x' = \text{FFN}(\text{LayerNorm}(x)) + \alpha \text{LayerNorm}(x), \quad \alpha \in [0, 1]$$

$$\text{LayerNorm}(x') = \gamma \frac{x' - \mu}{\sigma} + \beta$$

Then, a feed-forward network (FFN) is applied. The result is passed to another residual connection and norm layer.

## 4.6 Variational Auto-Encoders

The Variational Auto-Encoder (VAE) is a generative model introduced by Kingma and Welling (2013). VAE transforms the input data into a continuous latent space. It includes an encoder and a decoder. The encoder  $q_{\varphi}(z|x)$  learns to approximate the posterior distribution of latent variables  $z$  using input data  $x$ . The decoder  $q_{\theta}(x|z)$  learns to reconstruct the input data  $x$  using samples from this latent distribution. Typically, a standard normal distribution is used as the prior distribution  $p(z)$ .

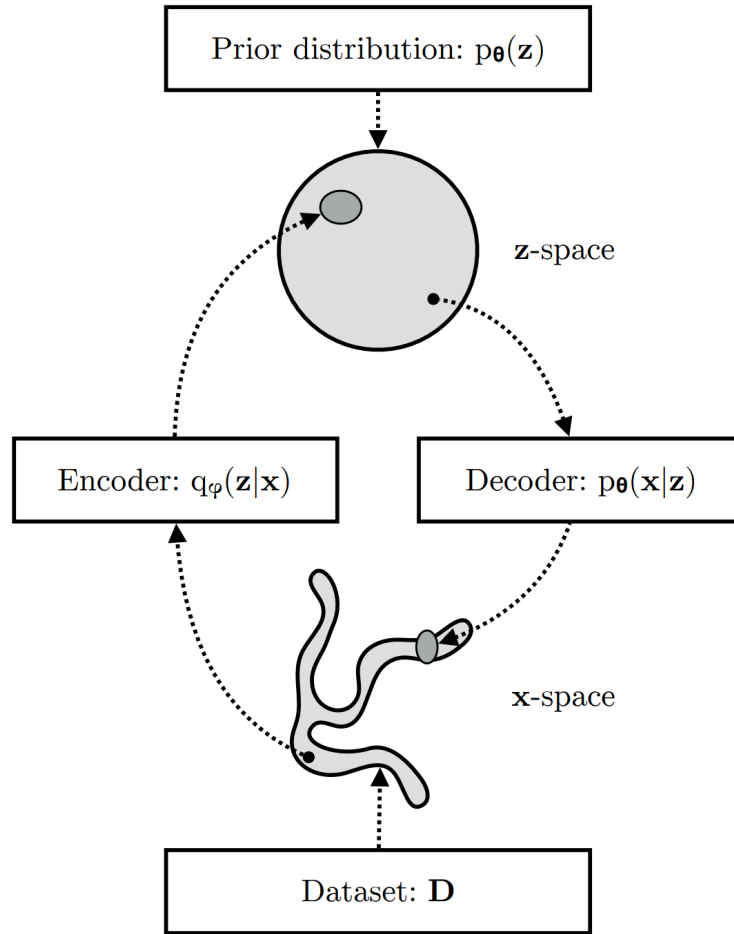


Figure 4.4: VAE architecture

$$\mathcal{L}_{\text{VAE}} = \mathcal{L}_{\text{MSE}}(x, \hat{x}) + \text{KL}(q_{\varphi}(z|x) || p(z))$$

$$q_{\varphi}(z|x) = \mathcal{N}(z; \mu_{\varphi}(x), \sigma_{\varphi}^2(x))$$

$$p(z) = \mathcal{N}(0, I)$$

$\varphi, \theta$  : learnable parameters

The loss function of VAE combines two terms: (1) the reconstruction loss, and (2) Kullback–Leibler divergence (KL divergence) loss. The first term is the loss function. It uses

Mean Squared Error (MSE) to ensure that the output data matches the input data. The second term is a regularization term (KL divergence) that pushes the latent distribution toward a standard normal prior. The encoder produces two learnable parameters for the latent space: mean  $\mu_\phi(x)$  and variance  $\sigma_\phi^2(x)$ .

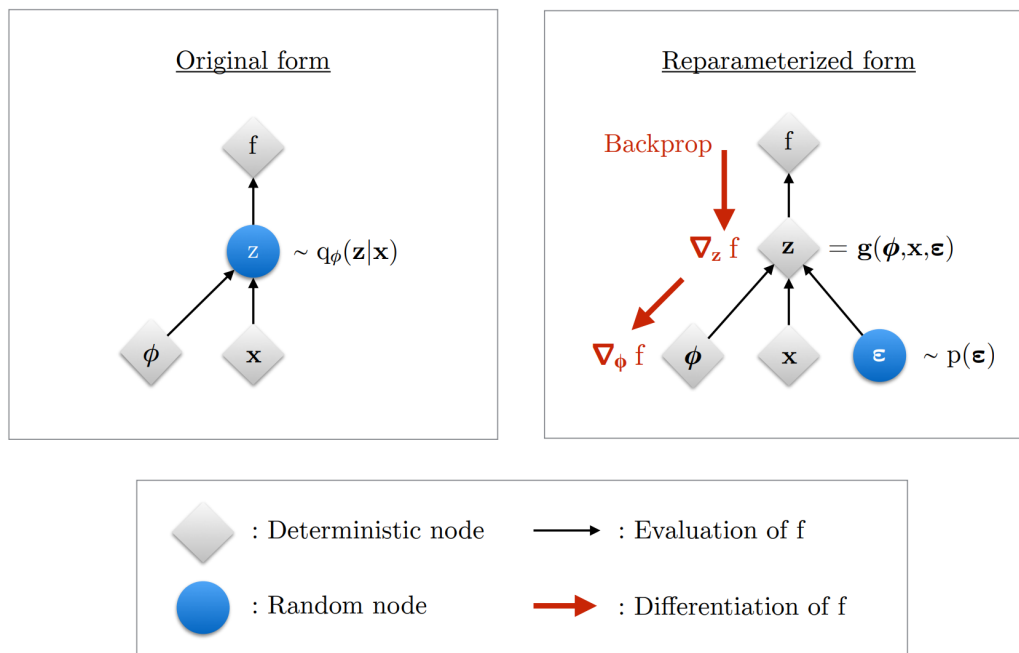


Figure 4.5: VAE reparameterization

Back propagation is impossible through the sampling process. To enable back propagation, VAE employs a reparameterization trick. Instead of directly sampling from  $q_\phi(z|x)$ , VAE samples  $\epsilon \sim \mathcal{N}(0, I)$  and then computes  $z = \mu_\phi(x) + \sigma_\phi(x) \odot \epsilon$ , where  $\odot$  refers to element-wise multiplication. By applying this reparameterization trick, VAE successfully converts the previously random sampling into deterministic and differentiable nodes of encoder parameter  $\phi$ , input data  $x$ , as well as random noise  $\epsilon$ . As a result, the latent embedding  $z$  can be expressed as

$$z = g(\phi, x, \epsilon)$$

## Chapter 5

# Experiment 1: Machine Learning Benchmarks

Based on annotated recording files, we extracted the onset and duration of each annotated syllable. In this experiment, we engineered different feature representations for each neuron in each annotated syllable, and used these features for syllable classification. This experiment aimed to establish the baseline performance on the classification of different syllables, identifying hub neurons, and investigating how neural information is integrated by the model through time.

### 5.1 Methods

#### 5.1.1 Feature Extraction

##### 5.1.1.1 Single Neuron Level

We first evaluated the predictive power of each neuron. For each neuron, we calculated firing rates during the entire syllable production. For each neuron, we trained classifiers using its firing rate.

### 5.1.1.2 Neuron Population Level

We analyzed the predictive ability of neurons on a population level to investigate the correlation and interaction between neurons in classification tasks. We used three types of feature representations. For each representation, we created a feature vector of length 75, which is equal to the number of neurons. Each element in the feature vector corresponds to one neuron’s activity. Each feature representation was independently evaluated using basic classifiers.

The first representation is the total number of spikes of the neuron per syllable. The second representation is the mean firing rate of the neuron per syllable. The third representation is Term Frequency-Inverse Document Frequency (TF-IDF). The TF-IDF indices were calculated by treating each neuron as an individual word and each annotated syllable as a document. Thus, the total number of firing during an annotated syllable sample served as the number of occurrences of the word in the document.

### 5.1.2 Models and Evaluation

For each of the feature representations above, we trained Support Vector Machine (SVM), Random Forest (RF) and eXtreme Gradient Boosting (XGBoost) classifiers. We evaluated the accuracy of each model for each feature representation. Then, we used three methods to evaluate the feature importance and interaction between neurons. The first is the built-in feature importance visualization method in RF, which identifies key contributing neurons. The second uses SHapley Additive exPlanations (SHAP) (Lundberg and Lee, 2017) values to identify the most important neurons for each syllable. The third is using SHAP interactive values to visualize pairwise interactions between neurons and find potential hub neurons. We first plotted a heatmap for all neurons and then picked top 10 interactive pairs and plotted them on a segment of Neuropixel. We also computed the spike rate correlation for comparison with SHAP interaction patterns. For the second and third methods, SHAP values were calculated using TreeSHAP for XGBoost models only. TreeSHAP is computationally efficient but does not support SVM or RF.

### 5.1.3 Neural Information Integration

Building upon our previous classification experiments, we conducted two analyses using SVM and population level mean firing rates to further investigate temporal relationships in our data.

The first analysis quantifies how different temporal segments contribute to classification performance. We performed a parameter sweep to analyze the accuracy of SVM trained on mean firing rates across different time periods. In this parameter sweep:

- Window start points vary from  $-200.0$  ms to  $-12.5$  ms
- Window end point increments by  $2.5$  ms, until it reaches  $100.0$  ms

For instance, the initial window would be  $[-200.0$  ms,  $-197.5$  ms], and the decoding accuracy using this data is stored. The second window would be  $[-200.0$  ms,  $-195.0$  ms], the accuracy is stored again. The window increases until it reaches  $[-200.0$  ms,  $100.0$  ms], where the accuracy is stored, and the second round starts with  $[-175.0$  ms,  $-172.5$  ms], and increases until  $[-175.0$  ms,  $100.0$  ms], etc.

The second analysis aimed to reveal spatially and temporally important patterns of information encoding in the neural population. To achieve this, another window sweep was done to extract fixed  $20$  ms windows between  $-150$  ms and  $50$  ms.

## 5.2 Results

### 5.2.1 Classification Accuracy

Table 5.1 shows the results of classification accuracy across different feature and models.

Feature Type	SVM (%)	RF (%)	XGBoost (%)
(Single Neuron) Mean Firing Rate	39.0	66.8	64.2
(Neuron Population) Total Spike Counts	91.5	89.6	96.2
(Neuron Population) Mean Firing Rates	77.3	91.7	91.2
(Neuron Population) TF-IDF	80.0	81.7	77.7

Table 5.1: Classification accuracy

### 5.2.2 Single Neuron Mean Firing Rate

From Figure 5.1, we can observe that neurons located at depths of 2000–3000  $\mu m$  have higher accuracies than the rest, but the overall variation across neurons of different depth remains small. The result from SVM suggests that the information is not encoded at single neuron level, and the decoding requires population level activity patterns. In the figure, each horizontal bar represents the classification accuracy using only that neuron’s firing rate as the predictor. The accuracy is also encoded by the color. Color and length were used together to separate the neurons recorded at the same depth. The x-axis shows the distance of each neuron to the tip of the Neuropixels probe in  $\mu m$ .

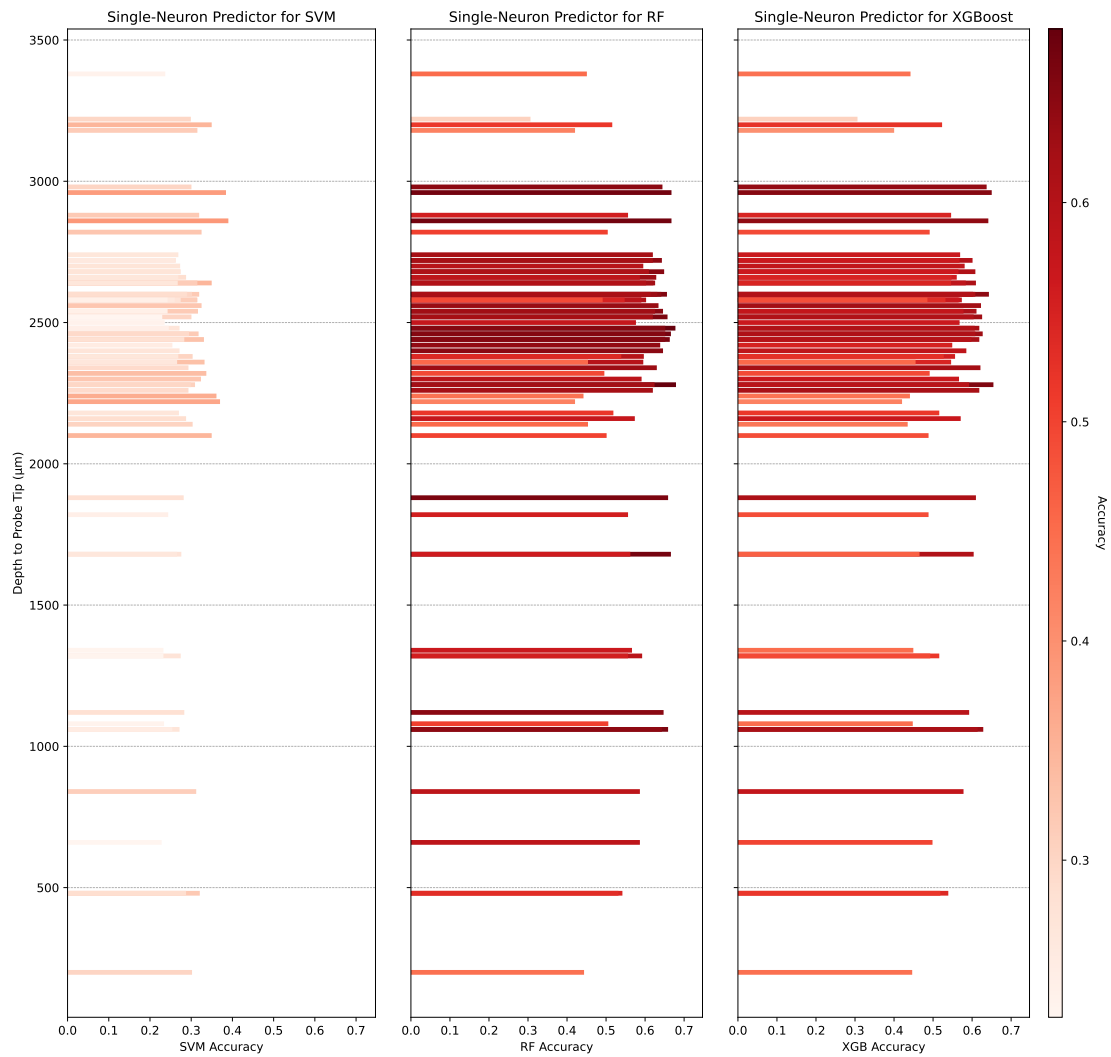


Figure 5.1: Classification accuracy using single neuron firing rates

### 5.2.3 Neuron Population Total Spike Counts

All classifiers achieved high classification accuracy using total spike counts for each syllable. However, this performance should be interpreted with caution. Some neurons exhibit consistent firing patterns, and may encode temporal information more than syllable-specific features. Since each syllable differs in duration, the result of classification using total spike counts may also reflect temporal characteristics across syllables of different lengths instead of syllable-specific neural activities. Figure 5.2 shows the feature importance, and how the most important neurons in Figure 5.2a are aligned with the total spike counts shown in 5.2b. This suggests that the RF simply learns the syllable length instead of focusing on genuine neural patterns.

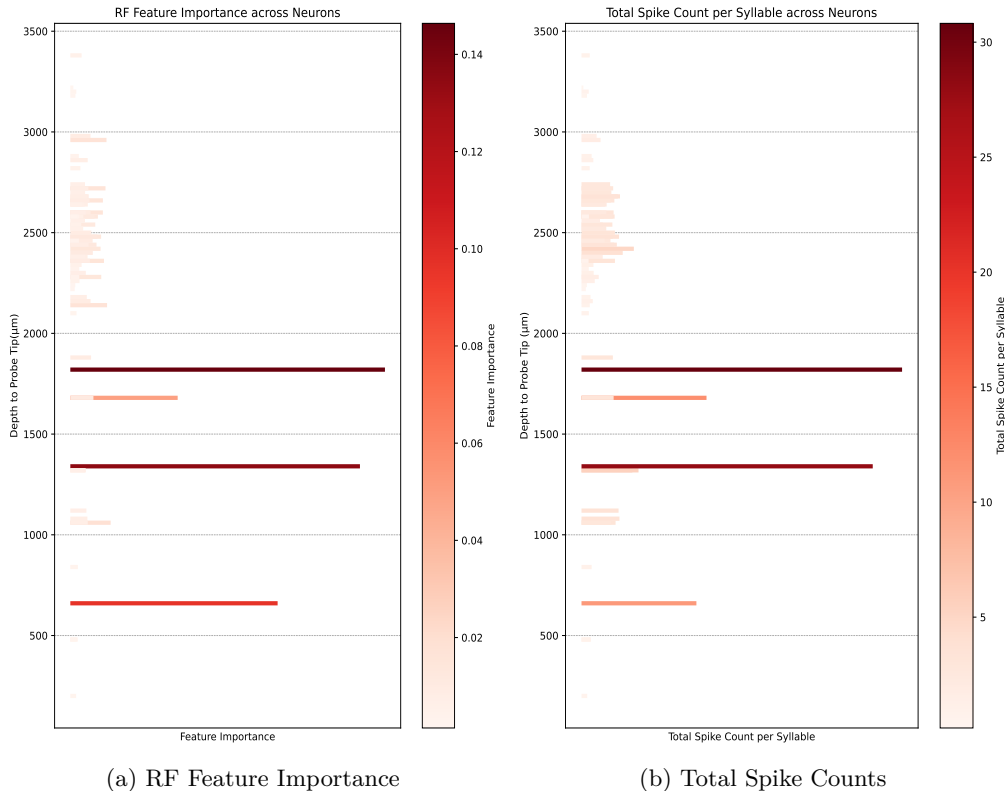


Figure 5.2: Evaluation of total spike counts

### 5.2.4 Neuron Population Mean Firing Rates

SVM achieved 77.3% accuracy while RF reached 91.7% accuracy using mean firing rates. Figure 5.3 shows the importance of each neuron during the classification task in

an RF model. Darker red indicates higher contribution to the correct classification.

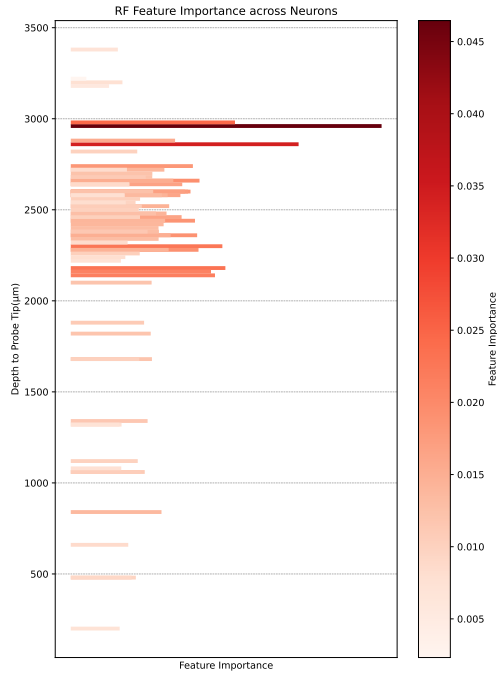


Figure 5.3: RF feature importance  
Mean firing rates

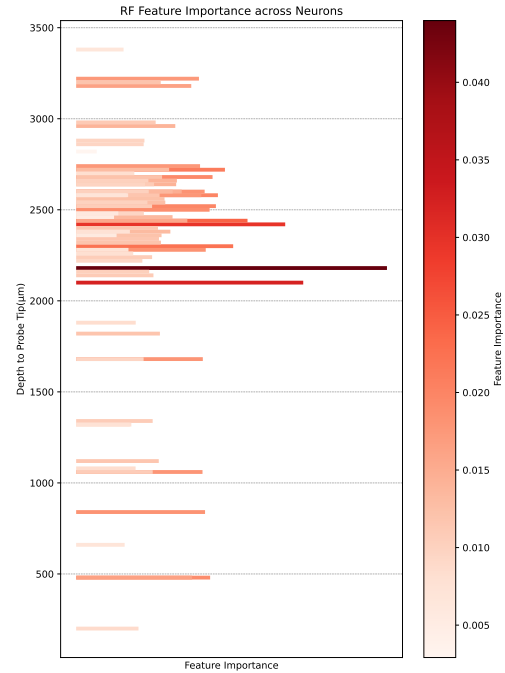


Figure 5.4: RF feature importance  
TF-IDF

### 5.2.5 TF-IDF

SVM achieved 80.0% accuracy and RF achieved 81.7% using TF-IDF as feature representations. Figure 5.4 visualizes the feature importance from the RF model.

### 5.2.6 SHAP Analysis

XGBoost classifier achieved a 91.2% accuracy. The result of XGBoost is visualized using SHAP visualizations to investigate the interaction between neurons. Figure 5.5 visualizes feature importance for each syllable using SHAP values. Higher SHAP values (darker red) indicate stronger positive contribution to the classification of specific syllables. The visualization shows distinct patterns of neuronal contributions to the correct identification of each syllable. Noteworthy the neuron N6 at depth 2960  $\mu m$  plays the most critical role among the classification of all syllables.

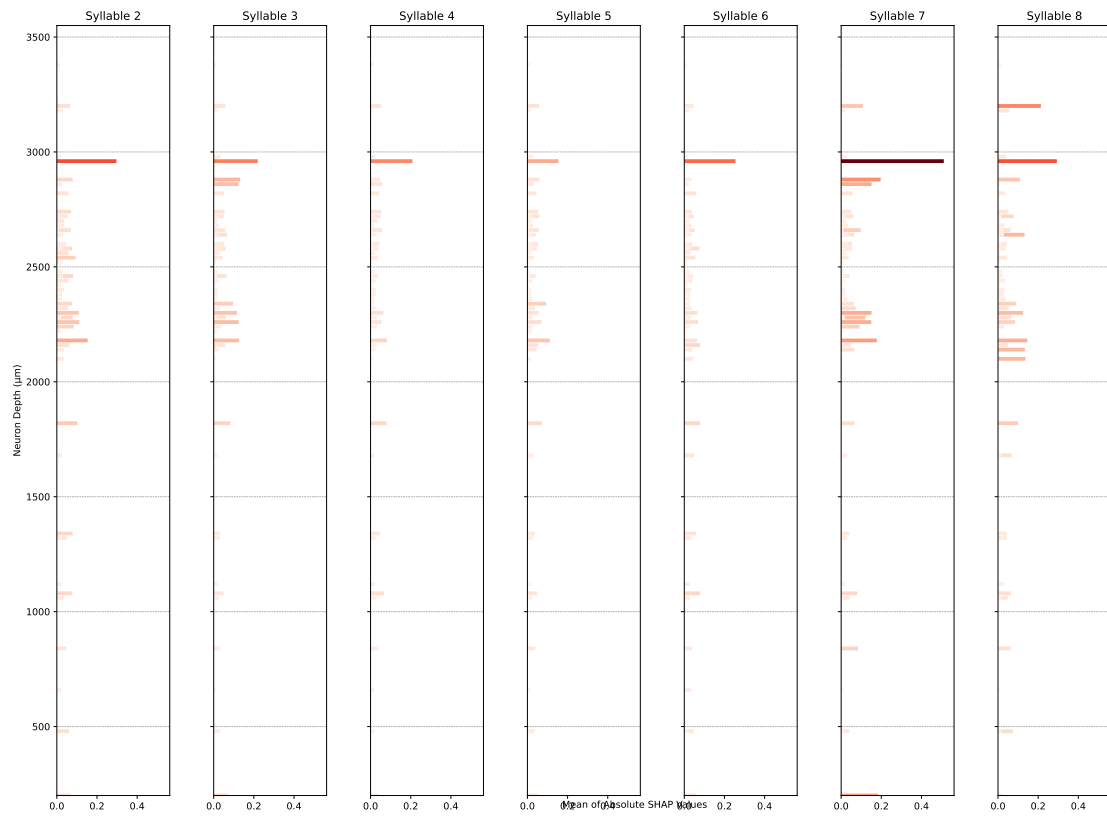


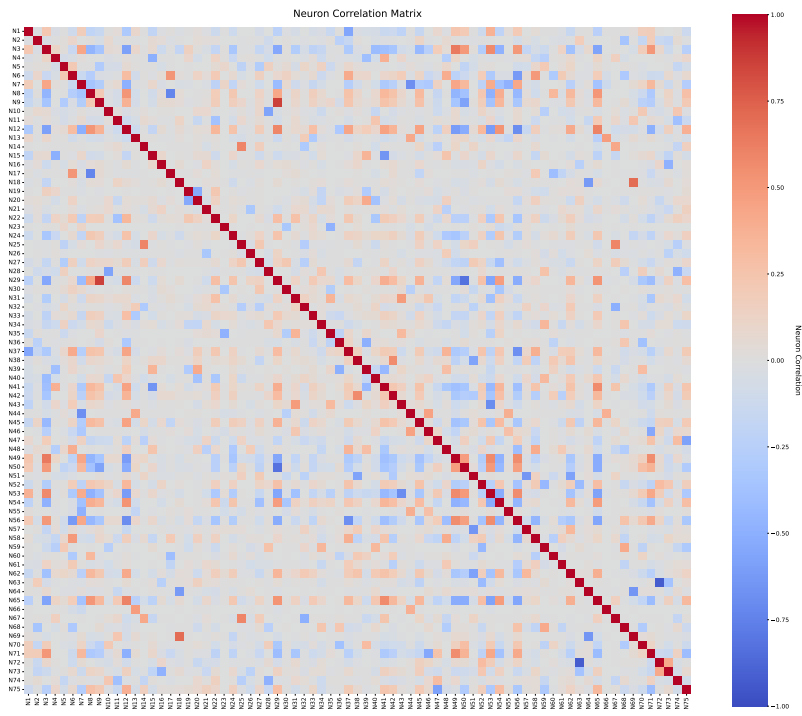
Figure 5.5: SHAP visualization of neuron importance for classification

### 5.2.7 SHAP Interaction Analysis

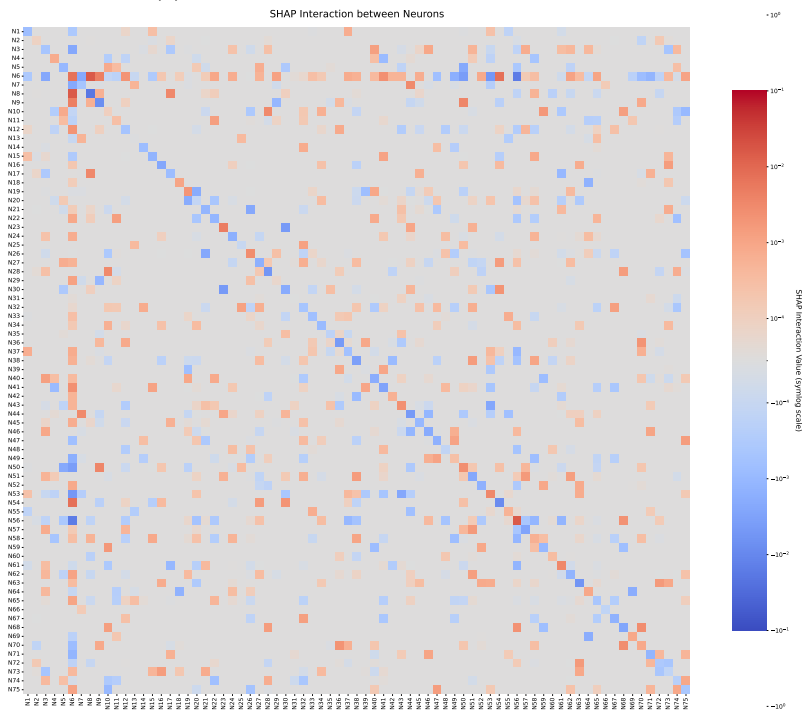
Figure 5.6a shows the correlation coefficients between neuron firing rates. Neurons N1(3380)–N12 (2720  $\mu m$ ) and N49(2320)–N56(2180  $\mu m$ ) show opposite firing patterns compared to other neurons during syllable production.

Figure 5.6b shows a heatmap of the relationship between the neurons calculated from SHAP interaction values. The neurons were inversely ranked by the depth to probe tip. A positive SHAP interaction value in red suggests that when both neurons are active, they contribute more to the syllable classification than the sum of individual contributions. A negative SHAP interaction value in blue suggests that when both neurons are active, their total contribution is less than the sum of their individual contributions. This could result from redundant information encoding, or potential inhibition effect from inhibitory interneurons. We can observe from the figure that Neuron 6 serves as a hub neuron. When it is active, it can either enhance (red dots) or suppress (blue dots) the contributions of other neurons to syllable classification, depending on the specific neural states. The depth of all neurons can be found in the appendix A.1.

The two figures show certain shared spectral patterns on the distribution of less correlated neurons (in gray). Additionally, Figure 5.7 visualizes the interaction of top 10 pairs of important neurons (called Features in the SHAP package) on a Neuropixels probe. The colored step lines indicate the interaction conditions between neurons. In the figure, N6 actively interacts with N8 and negatively interacts with N56. N6 and N8 are roughly located on the edge of LMAN, while N56 is roughly located at area X.



(a) Correlation coefficients between 75 neurons



(b) SHAP visualization of interactions between neurons  
 Figure 5.6: Neural correlation and interaction analysis

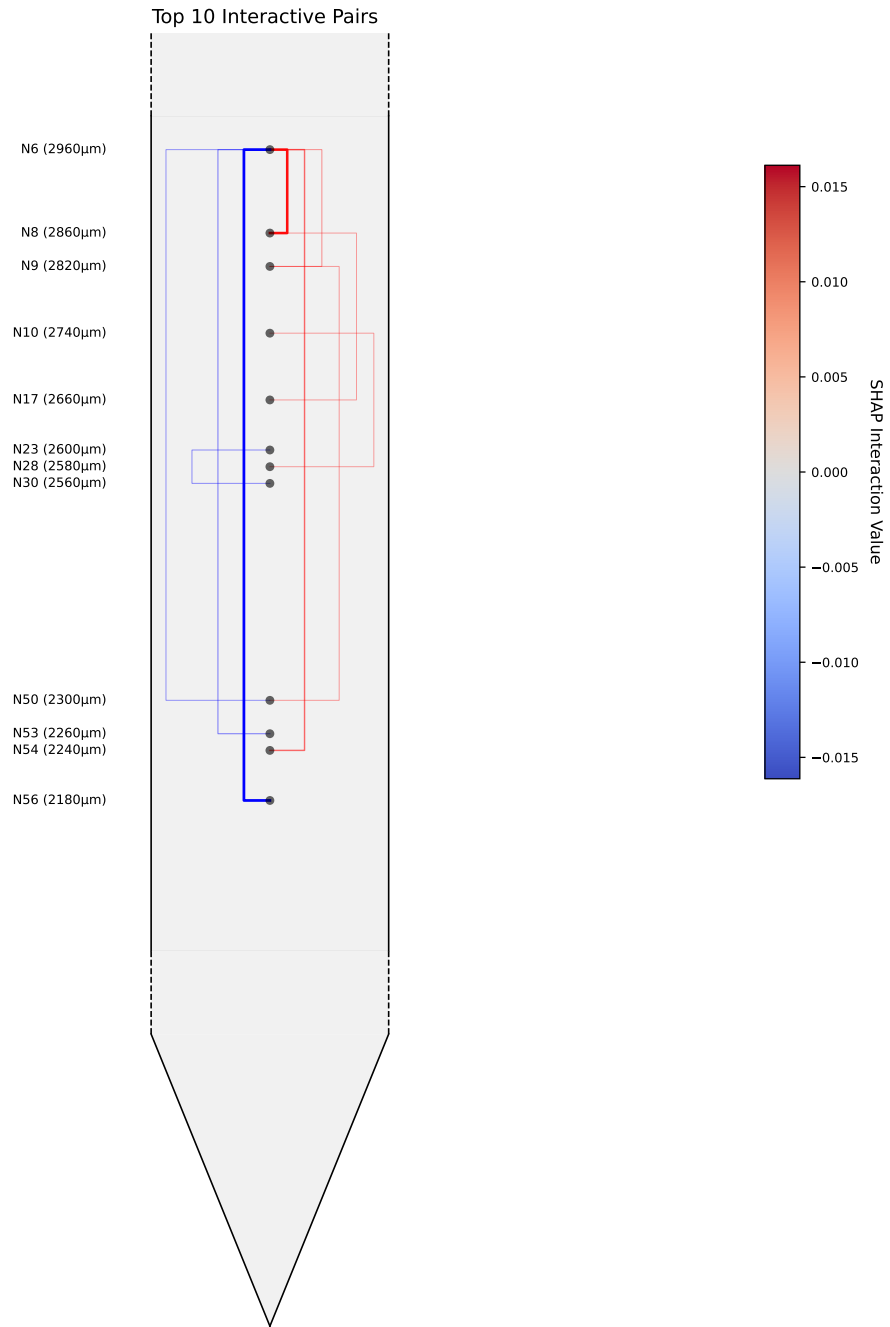


Figure 5.7: Top 10 interactive pairs plotted on a Neuropixels probe

### 5.2.8 Neural Information Integration

Figure 5.8 shows the decoding accuracy using the mean firing rates of neuron population using a basic SVM.<sup>1</sup>

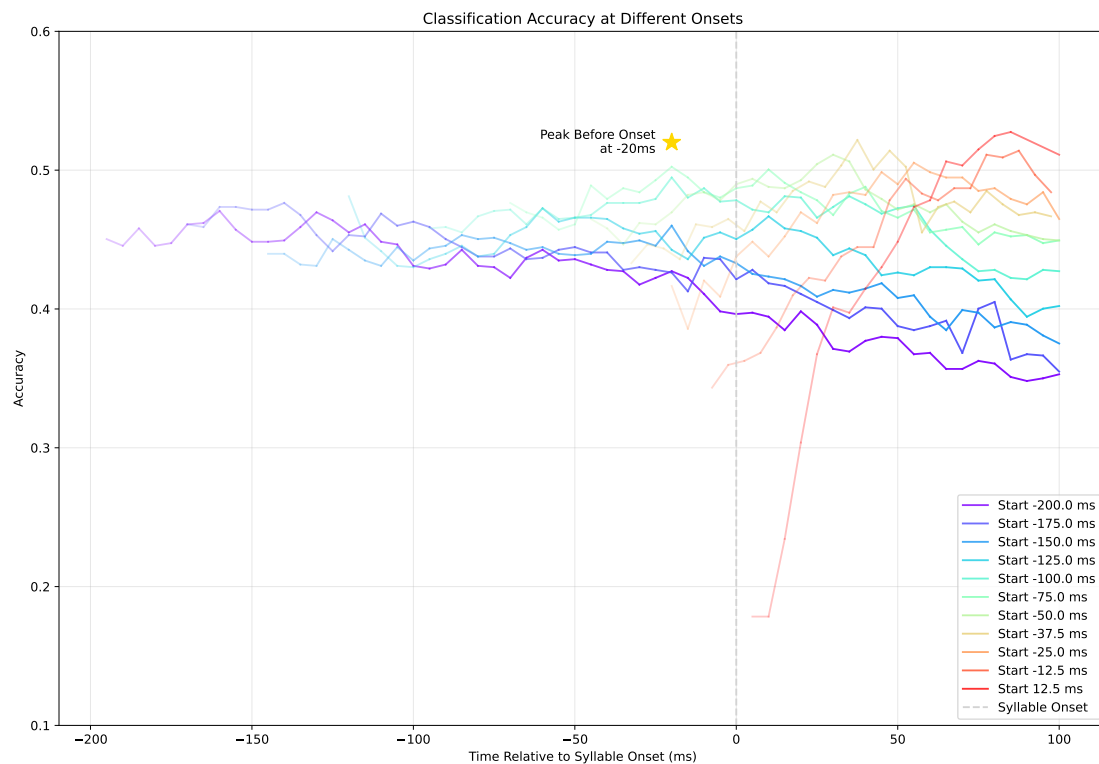


Figure 5.8: Classification accuracy

Each colored line indicates how classification accuracy evolves when integrating neural activity from a specific starting point. The transparency indicates the total length of windows used for classification. For instance, the purple line starts at  $-200$  ms. It collects the spikes every  $5$  ms, and uses these spikes to do classification. The first point in the purple line at  $-195$  ms indicates the classification accuracy using spikes collected during  $[-200$  ms,  $-195$  ms]. Then it collects the spikes during  $[-200$  ms,  $-190$  ms], and the accuracy is reflected by the value of the purple line at  $-190$  ms.

On the other hand, highest classification accuracies occur at  $-20$  ms. Colored lines starting at  $-12.5$  ms show very low accuracy, which indicates that there are homogeneous

<sup>1</sup> Individual plots of each onset is included in Appendix A.2

activities in all syllables around the syllable onset. Based on this observation and inspired by Multivariate Pattern Analysis in EEG, we did the second analysis.

In the second analysis, we binned the firing counts into 2.5 ms windows in the range  $[-150 \text{ ms}, 30 \text{ ms}]$  and use these as input features to an RF model. Figure 5.9 visualizes the feature importance. There are occasionally dark red dots between  $[-50 \text{ ms}, -25 \text{ ms}]$  before the onsets, indicating these time windows contain relatively more important information for correct identification of syllables.

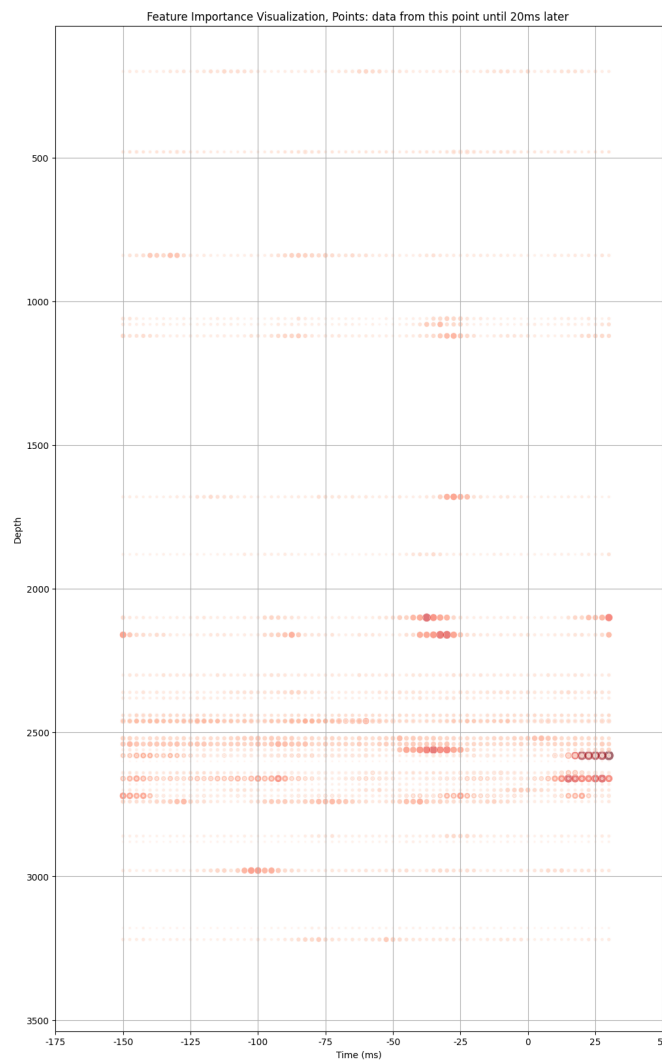


Figure 5.9: Classification performance in different random time windows

## 5.3 Discussion

### 5.3.1 Baseline Methods and Interpretation

Our benchmark results show that the mean firing rates can be used to classify different syllables of zebra finches. A fair baseline can be established by passing mean firing rates on a neuron population level to SVM, yielding an accuracy of 77.3%. RF and XGBoost have better results, but may come from brute force ensemble averaging rather than understanding true data patterns. Individual neurons show some predictive power, and the population level features suggest that the syllable is mostly encoded at the population level. In addition, TF-IDF is a useful metric and yields a high classification accuracy. SHAP analysis revealed two findings: syllable-specific patterns in neural activity, and neuron interactions. The analysis identified important neuron hubs, and visualized possible relationships between neurons in LMAN and area X.

### 5.3.2 Information Encoded in LMAN Activity

The first neural information integration analysis suggests that LMAN activity at  $-20$  ms is the most informative for syllable classification. The second analysis showed that during  $[-50$  ms,  $-25$  ms], the LMAN activity is the most informative for the vocalization of different syllables. These temporal relationships align well with previous findings of LMAN's pre-motor activity during syllable production. Previous studies have reported LMAN pre-onset bursts occurring at  $[-60$  ms,  $-10$  ms] (Kojima et al., 2018),  $[-42$  ms,  $-20$  ms] (Giret et al., 2014), and  $-50$  ms (Kao et al., 2005).

### 5.3.3 Future Direction

The results indicated LMAN activities contain important timing-specific information around syllable onset. A systematic temporal windows analysis could reveal more precise patterns of information encoding in LMAN. The SHAP interaction analysis and the information integration analysis can be applied to data from HVC and RA, enabling visualization of information flow and integration between AFP and Motor Pathway. The method could also be used on simultaneously recorded data from Area X and DLM to investigate the GABAergic projection from Area X to DLM. These analyses would advance our understanding on how Motor Pathway and AFP coordinate and contribute

to motor output from a machine learning perspective.

## Chapter 6

# Experiment 2: Token-based Deep Learning Methods

This experiment aimed to process neural data using NLP methods. The spike data were converted into text tokens in the NLP framework.

### 6.1 Methods

#### 6.1.1 Tokenization Method

We passed in binary data in a text format. For each sampling time, the data were then combined across all 75 neurons from the shallowest to the deepest. For binary data, each value was either 1, which indicates a firing, or 0, which indicates non-existence of firing. Each text token would then be composed of 75 binary values. Data representing one sampling time (0.05 ms) is shown below:

$$\underbrace{\langle \text{START} \rangle}_{\text{bos}} \underbrace{0000100000 \dots 0000000010}_{75 \text{ Neurons}} \underbrace{\langle \text{END} \rangle}_{\text{eos}}$$

The first 0 refers to neuron 1 being inactive, and fifth 1 refers to neuron 5 being active. The neurons are re-indexed according to their depth to probe tip from small to large.

We collected all such combinations, and used Byte-Pair Encoding (BPE) to train a

tokenizer. The goal was to represent each sampling time by one input token ID. Since BPE creates both complete units and subunits with varying lengths, we aimed to keep only complete tokens with a length of 75 (which is equal to the number of neurons). Since the tokenizer was trained on all possibilities, it automatically prioritized single complete tokens over multiple subunit combinations. Thus in practice, the incomplete subtokens had no impact on performance and were kept in the vocabulary. Figure 6.1 shows how the data were tokenized.

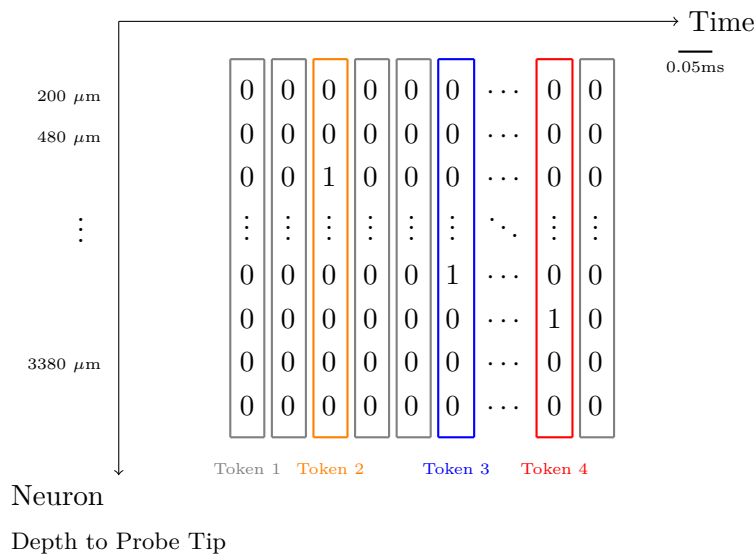


Figure 6.1: Transforming neural data in sampling time into tokens

We then used this tokenizer to tokenize the whole data, and we added three special tokens: (1) begin of sequence (bos) token  $\langle |START| \rangle$ , (2) end of sequence (eos) token  $\langle |END| \rangle$ , and (3) divider  $\langle | \rangle$ . The divider  $\langle | \rangle$  was used to combine multiple sampling times together. A data for two sampling times (0.1 ms) combined together looks like:

$$\langle |START| \rangle \underbrace{0000100000\dots0000000010}_{\text{Data 1}} \underbrace{\langle | \rangle}_{\text{divider}} \underbrace{0000000000\dots0010000000}_{\text{Data 2}} \langle |END| \rangle$$

This tokenization method allowed us to represent binary spike train data into limited numbers of tokens for subsequent analysis. The obtained vocabulary size is 4087 (7107 including subunits), and  $\approx 90\%$  of the data is empty data consisting of 75 zeros.

### 6.1.2 Data preparation

We used the following data lengths: 0.05 ms (with and without empty tokens), 0.5 ms, 1.5 ms, 2.5 ms, 3 ms, 5 ms, 6 ms, 15 ms, 30 ms, 45 ms, and 60 ms. Since 60 ms exceeded the lengths of some annotated syllables, padding was introduced to maintain consistent input dimensionalities.

### 6.1.3 Models and Evaluation

We randomly initialized the weights of two Hugging Face models to borrow their mature structures. The first model is OpenAI GPT-2 model (Radford et al., 2019) with 142M parameters, and the second model is a Mamba (Gu and Dao, 2023) model with 130M parameters with a sequence classification head. The models were evaluated using classification accuracies across different data lengths and model architectures. We then compared the best performing model against our previously established SVM benchmark.

## 6.2 Results

### 6.2.1 GPT-2 performance

Table 6.1 and Figure 6.2 show the classification accuracy of GPT-2 increases with input data length from 15 ms, and reaches 47% with information from 60 ms. On the other hand, data shorter than 15 ms failed for the task, even when the sparsity was removed.

Time (ms)	Accuracy (%)
15.0	38.5
30.0	41.6
45.0	44.8
<b>60.0</b>	<b>47.0</b>

Table 6.1: GPT-2 classification accuracy with sequences from 15 ms to 60 ms

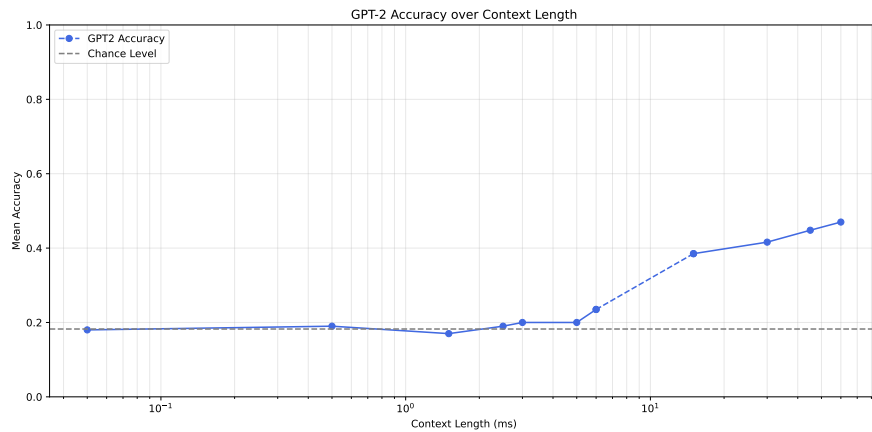


Figure 6.2: Performance of GPT-2

### 6.2.2 Mamba performance

Figure 6.3 shows that Mamba 130M failed the task with sequence length 45 ms.

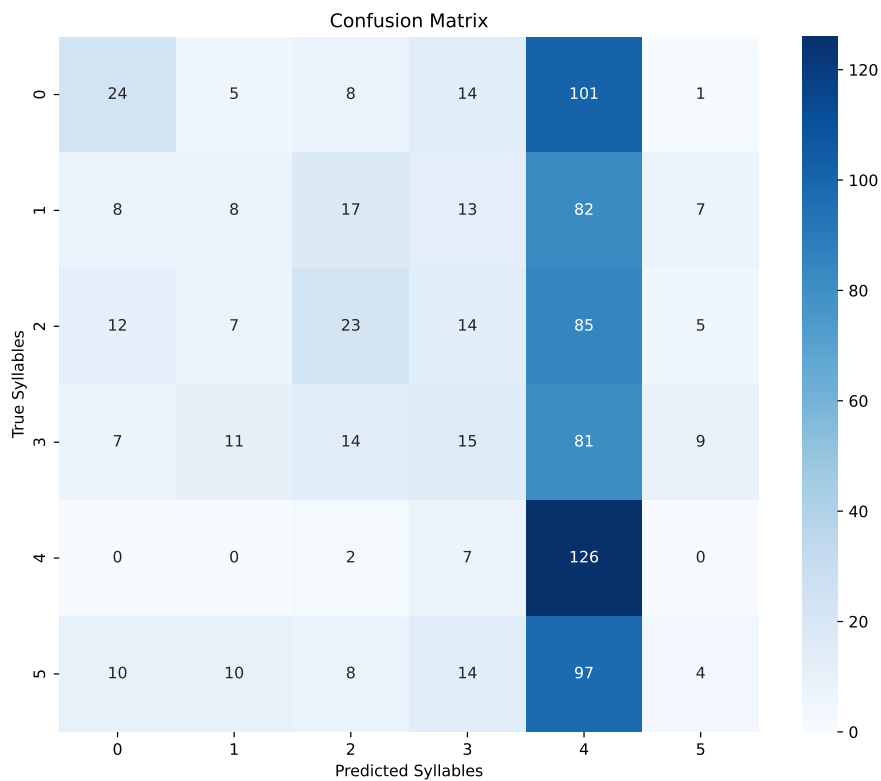


Figure 6.3: Mamba confusion matrix with 45 ms sequences

## 6.3 Discussion

### 6.3.1 Achievements on GPT-2 performance

Figure 6.2 shows the potential of GPT-2 in neural decoding tasks. The performance of the model increases to 47.0% with longer input sequence length. Our findings demonstrate the validity of the approach for transformers to deal with neural data as text tokens.

### 6.3.2 Limitations

The performance of GPT-2 model is not optimal. The final accuracy of 47% is below our established SVM benchmark 77.3% using mean firing rates. Additionally, the small Mamba model failed to decode 45 ms length data. The performance of large language models indicate that more data is needed.

### 6.3.3 Future Directions

The current decoding accuracy can be improved by training with data from the motor pathway instead of AFP. In addition, a pre-trained model could be developed using synthesized (Zhou and Wei, 2020) or open (de Vries et al., 2020) data from other animals and experiment paradigms, and then fine-tuned using real vocalization data. Introducing mixed transformer-mamba layers (Lieber et al., 2024) is also a promising approach to enhance the decoding accuracy.

## Chapter 7

# Experiment 3: Temporal Deep Learning Methods

This experiment explored deep learning architectures for syllable classification using neural data. We compared the performance of different neural network architectures (CNN-LSTM, EEGNet, LSTM, and Mamba-2) against the benchmark established from previous experiments. Both sampling time binary data and binned data were evaluated. We adopted the newly released Mamba-2 architecture (Dao and Gu, 2024) rather than the original Mamba (Gu and Dao, 2023), as Mamba-2 is computationally more efficient during training.

### 7.1 Methods

#### 7.1.1 Data

Data was selected around the onset using a moving window. Raw data in its original format [neuron, sampling time] were used as binary data. We also binned the binary values and tested various bin sizes, ranging from 0.1 ms to 20 ms. We picked corresponding windows using a parameter sweep, such that different windows around the onset could be picked and compared. The step size was fixed at 1.

For the parameter sweep, we tested bin sizes from 0.05 ms to 20 ms. For each bin size, we tested different temporal windows relative to syllable onset:

- pre-onset: from  $-125$  ms to  $0$  ms, incrementing by  $12.5$  ms
- post-onset: three values  $37.5$  ms,  $50.0$  ms, and  $62.5$  ms

The sequence length is determined by total time window length (ranging from  $37.5$  ms to  $187.5$  ms, computed as the sum of absolute values of pre-onset and post-onset times) and the bin size (ranging from no bin, which is  $0.05$  ms, to  $20$  ms). As a result, sequence lengths varied by up to three orders of magnitude, primarily driven by the bin size. When using original binary data or small bin sizes, the resulting data was considerably sparser when compared to those data processed with larger bin sizes.

### 7.1.2 Models and Evaluation

We used a two-layer LSTM model, a parallel CNN-LSTM model, a two-layer Mamba-2 model, and CNN-based EEGNet (Lawhern et al., 2016). The models were evaluated by classification accuracies across different pre-onset and post-onset parameters, bin sizes, and model architectures. The results were then compared against results in previous experiments.

## 7.2 Results

All models but EEGNet successfully completed the parameter sweep analysis. EEGNet encountered memory constraints when processing smaller bin sizes due to long sequence lengths. For the  $10$  ms bin size, we were only able to test pre-onset windows of  $-125$  ms and  $-112.5$  ms due to technical limitations. We therefore focused our bin size analysis on a single parameter combination (pre-onset:  $-125$  ms, post-onset:  $62.5$  ms). The overall trends remained consistent across other parameter combinations, indicating that this partial testing did not affect the reported observations. Results from the parameter sweep are presented below.

### 7.2.1 Top-3 Results for Each Model

The Top-3 results for each model are included in Table 7.1. EEGNet achieved a peak decoding accuracy of  $89.0\% \pm 1.7\%$ , with a bin size of  $15$  ms, a step size of  $0.05$  ms, and data extracted from  $-125$  ms to  $62.5$  ms.

Model	Bin (ms)	Pre-onset (ms)	Post-onset (ms)	Accuracy (%)
LSTM	2.5	-112.5	67.5	50.4 ± 1.9
	3.8	-125.0	67.5	50.3 ± 1.1
	5.0	-125.0	67.5	50.3 ± 1.2
Mamba-2	5.0	-125.0	67.5	57.7 ± 1.4
	10.0	-125.0	67.5	57.7 ± 1.2
	10.0	-112.5	67.5	57.1 ± 1.5
EEGNet	<b>15.0</b>	<b>-125.0</b>	<b>67.5</b>	<b>89.0 ± 1.7</b>
	10.0	-125.0	67.5	88.6 ± 0.5
	7.5	-125.0	67.5	88.3 ± 0.8
CNN-LSTM	7.5	-125.0	67.5	58.0 ± 0.8
	5.0	-125.0	67.5	58.0 ± 1.7
	5.0	-112.5	67.5	57.9 ± 1.0

Table 7.1: Top-3 parameter combinations for each model on accuracy

### 7.2.2 Model Performance Across Different Windows Periods

Figure 7.1 shows the performance of models with different pre-onset and post-onset combinations. Each grouped column represents one pre-onset time. Within each group, there are three connected data points showing the classification accuracies using different post-onset times.

The grouped columns of pre-onset times show a pattern from left to right. As the pre-onset time moves closer to the syllable onset, the classification accuracy decreases. Within each group, three connected dots of post-onset times form an ascending line. Larger post-onset time on the right consistently outperforms smaller post-onset time on the left.

In conclusion, longer data windows in both pre-onset and post-onset directions improve the decoding accuracy. This improvement appears stronger in shorter data, as shown on the right side of the figure. EEGNet has the best performance in all windows, and demonstrates the strongest sensitivity to data duration.

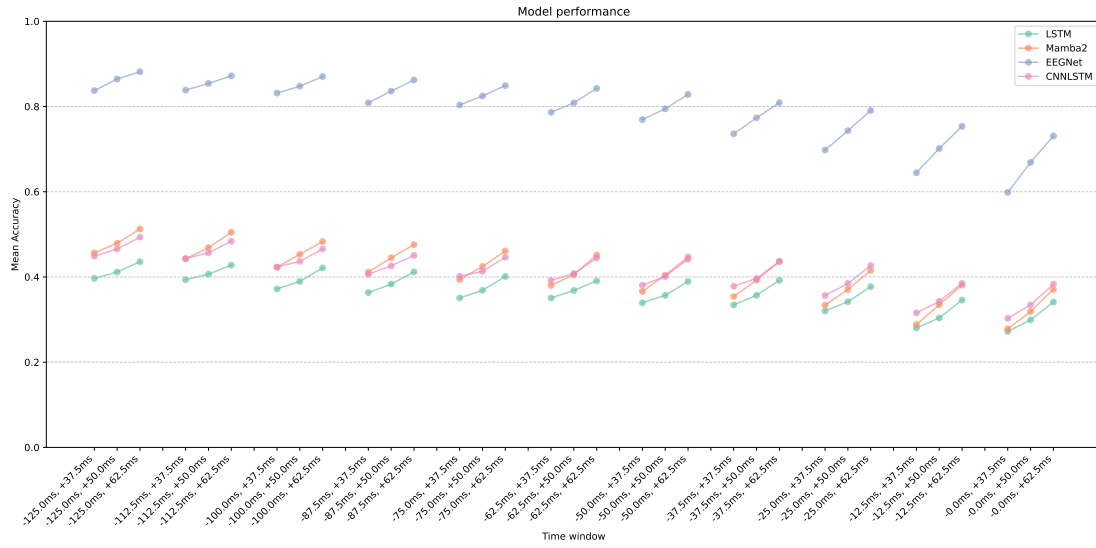


Figure 7.1: Model performance across different window periods

### 7.2.3 Model Performance Across Different Bin Sizes

Figure 7.2 shows the performance across different bin sizes. The time window used is  $[-125 \text{ ms}, 62.5 \text{ ms}]$ . The performance improves as bin size increases until the bin size hits 1.5 ms. Mamba-2 shows a better performance in small bin sizes.

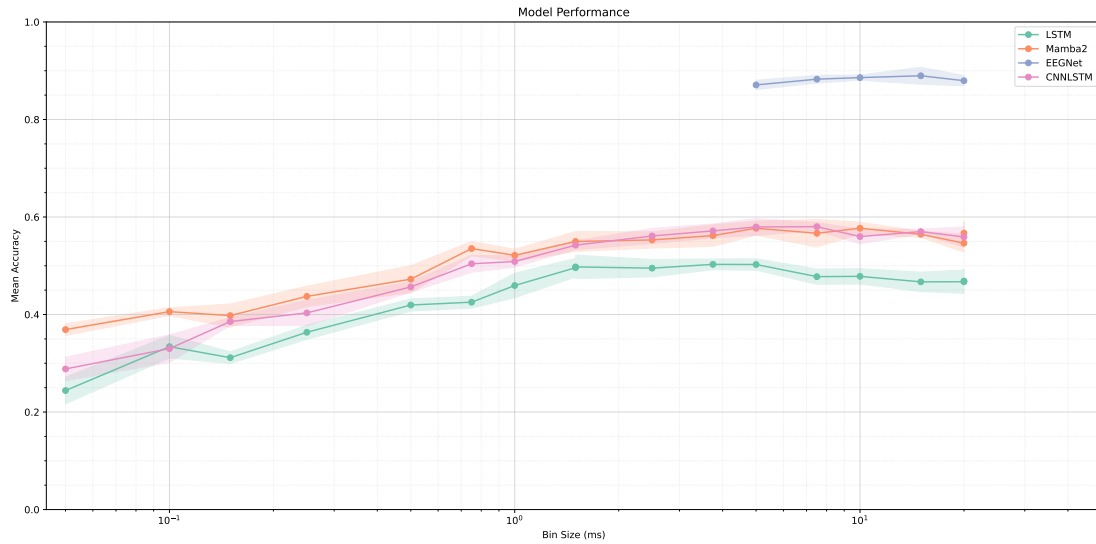


Figure 7.2: Model performance across different bin sizes

## 7.3 Discussion

### 7.3.1 EEGNet Performance on Binned Spike Data

Our results show that EEGNet’s architecture, originally designed to deal with the temporal and spatial characteristics of EEG recordings, successfully transfers its effectiveness to spike data analysis. It achieves a decoding accuracy of 89.0%, surpassing the 77.3% benchmark previously established in Experiment 1. The results suggest that deep learning models can effectively capture the complex patterns in neural spike data.

### 7.3.2 Effect of Binning

The performance increase until 1.5 ms bin size can be attributed to reduction in data sparsity and decrease in input sequence length. The performance plateau for all models beyond the 1.5 ms threshold indicate that this bin size achieves a balance between data sparsity, input sequence length, and fine-grained neural patterns. This plateau point at 1.5 ms aligns with the typical duration of an action potential (1–2 ms), suggesting that bin sizes beyond the timescale of individual spikes provide no significant benefit for performance. Different bin sizes have been used in literature, such as 1 ms, 8.33 ms, and 25 ms (Schneider et al., 2023; Zhou and Wei, 2020), reflecting data-specific choices that balance trade-offs between fine-grained temporal patterns and computational efficiency.

### 7.3.3 Limitations on Model Performance

Other models we implemented were less effective at capturing information in the neural data. Their best decoding accuracies are lower than the benchmark from Experiment 1. With sampling time data, their performances are also lower than the NLP methods, as shown in Table 7.2.

Model	Accuracy (%)
<b>GPT-2</b>	<b>47.0</b>
Mamba-2	26.2
CNN-LSTM	24.8
LSTM	21.1

Table 7.2: Model performance on sampling time

### 7.3.4 Future Directions

Mamba-2 showed some potential for dealing with the sparsity and long-range dependencies inherent in unbinned spike train data while maintaining computational efficiency. Future work could explore more sophisticated Mamba-2 architectures optimized for unbinned spike train data, and Conv2D layers could be incorporated to enhance the spatial pattern recognition capabilities.

## Chapter 8

# Experiment 4: CEBRA Latent Embeddings

Consistent EmBeddings of high-dimensional Recordings using Auxiliary variables (CEBRA) is a contrastive learning method to compress time series data and reveal its hidden structures (Schneider et al., 2023). The model can be self-supervised by temporal adjacency of neural activity, or supervised by behavioral labels, or both. CEBRA consistently generates interpretable latent embeddings in (1) synthesized spikes (Zhou and Wei, 2020), (2) hippocampal place encoding (Grosmark and Buzsáki, 2016), (3) somatosensory cortical activity during reaching (Chowdhury et al., 2019), and (4) visual cortical responses to videos (de Vries et al., 2020). We expect CEBRA to reveal the underlying structure of LMAN activity during vocalization as well. With annotated syllables, the neural data can be supervised by a simple categorical system of 7 syllable types. Thus we investigated the potential of latent embeddings produced by CEBRA for syllable classification.

### 8.1 Methods

#### 8.1.1 Data

We extracted the neural activity during the vocalization periods, and binned the data using a 10 ms window. Although this method interrupted continuous neural signals,

it allowed us to focus on the neural activities of interest. Prior to concatenating, we shuffled the data at the syllable level to break the natural sequence of song.

### 8.1.2 Models

CEBRA learns patterns in five ways:

1. over time
2. over label
3. over label, shuffled on a label level so that the labels are not in original order
4. over label, shuffled on a sample level
5. hybrid, jointly over time and label

We focused on exploring the hyperparameter ‘offset’ which defines the distance (in time) between positive pairs (Schneider et al., 2023). A positive pair is composed of two timepoints separated by the offset value. Time points outside this interval become negative pairs. For example, an offset of 10 refers to the fact that time point  $t \pm 10$  form positive pairs, and time point outside of this period will be used as negative pairs. Lower offset values lead to more stable learning, since temporally adjacent neural activities are more correlated. Higher offset values might lead to less stable learning, as the temporal correlation between neural activities decreases with longer time intervals.

In the experiment, the dimension of latent embedding is set to 3, the learning rate is set to  $3e - 4$ , the number of epochs is dynamically adjusted between 5000 to 50000 by observing the training loss. Train-test split was 8–2. The model was trained on the training set and we obtained the final embeddings by passing all data (including the test set) through the trained CEBRA model.

### 8.1.3 Evaluation

Our evaluation process consisted of three steps. First, we visualized trained embeddings<sup>2</sup> to evaluate how data points from different labels distributed in the embedding space.

---

<sup>2</sup> Only the third model is visualized in the experiment. Appendix A.3 shows the visualization for four other models, their training loss, and data distribution.

Second, we performed single time point classification. We passed individual CEBRA embeddings to SVM, RF, and XGBoost, and compared the best result to benchmarks from Experiment 1 using total count of spikes over 10 ms. By doing this, we ensured that we were comparing the same temporal resolution of 10 ms. The performance of all the models, including the ones in the Appendix, were included in the classification accuracy table.

Finally, the latent embeddings were evaluated using sequence classification. For this, we combined the embeddings into sequences, and applied CNN-LSTM to these sequences. Identical window and parameters of data processing from Experiment 3 were used in the comparison. The CNN-LSTM was picked due to its ease of implementation and its potential for further improvement with enhanced input features.

## 8.2 Results

### 8.2.1 Visualization of CEBRA latent embeddings

Figure 8.1 visualizes the latent embeddings of all binned data, generated by CEBRA model trained on shuffled syllables.

The visualization shows excellent clustering with parameter offset 10 and offset 20, where the latent embeddings form a circular pattern. The spatial arrangement of neural data in the embedding space preserves their original sequence order in songs, despite the fact that the syllables are shuffled. The boundaries between different syllables appear to be thin and discontinuous. In comparison, unshuffled data in Appendix A.3 shows more distinct boundaries between syllable regions.

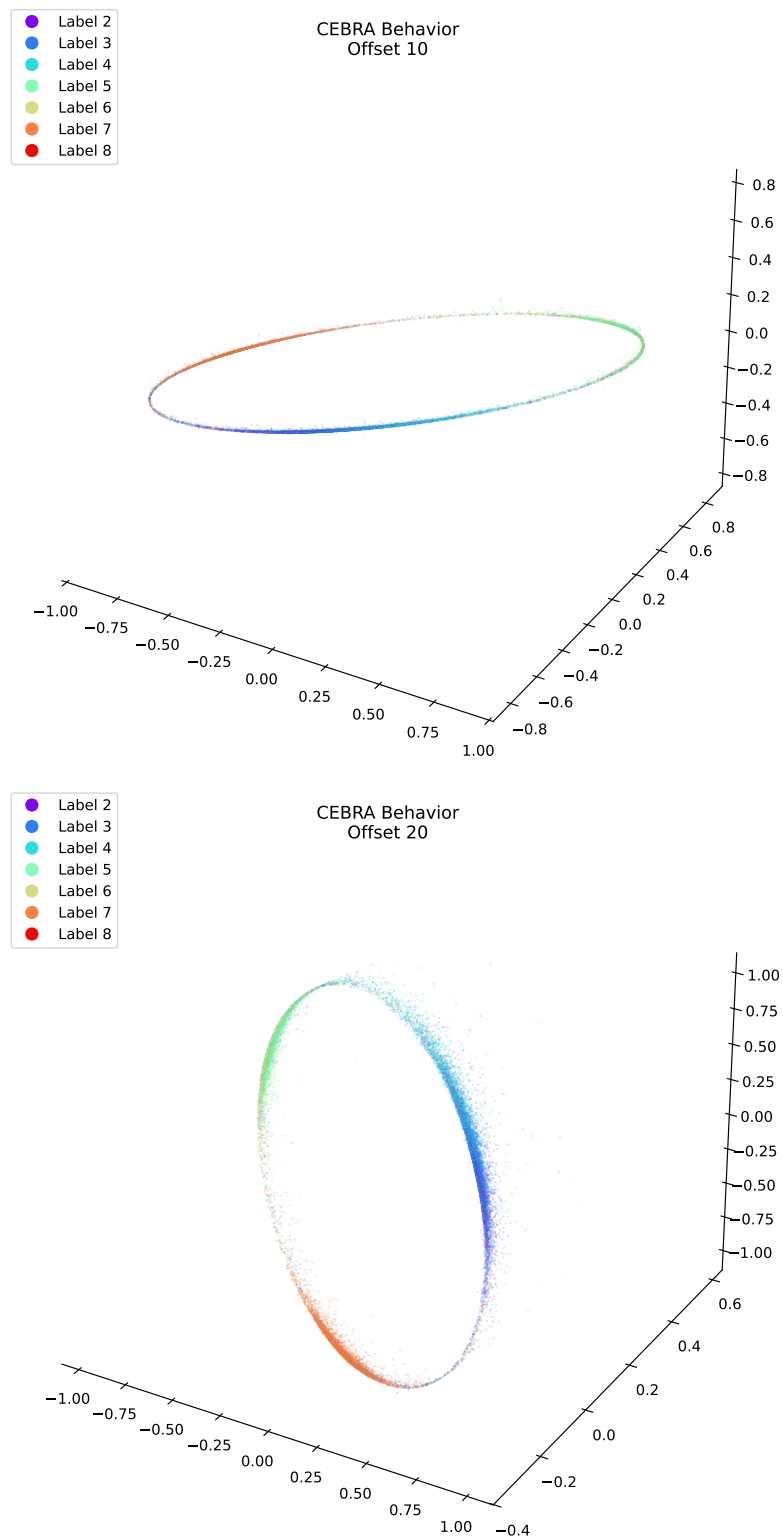


Figure 8.1: CEBRA embeddings trained with shuffled behavior labels

### 8.2.2 Single Time Point Classification

CEBRA assigns each labeled neural data point (obtained by binning the spikes over 10 ms) a 3-dimensional latent embedding. We passed these latent embeddings to three classifiers: SVM, RF, and XGBoost. Table 8.1 shows the results for all models<sup>3</sup>. The behavior models achieved the best classification performance, and larger offset parameter increases the model performance. The result visualized previously is the third model: Behavior shuffled over labels. The best result is 64.2% with parameter offset 20.

The result from the behavior models outperformed the baseline method. Using the same 10 ms window size, we tested the classification accuracy by counting the total number of spikes during fixed 10 ms windows as features to the same SVM. The best accuracy was around 36.7% from time window  $[-20 \text{ ms}, -10 \text{ ms}]$ , which is well below the result obtained using CEBRA latent embeddings.

### 8.2.3 Sequence Classification

We applied the CNN-LSTM model from Experiment 3 to sequences of CEBRA embeddings, and obtained an accuracy of 81.8%. The embeddings were from behavior models with shuffled labels and an offset of 10.

Table 8.2 shows CNN-LSTM with CEBRA embeddings outperforms the same CNN-LSTM using binned spikes. The data had a similar window size and the models have the same structure. The CNN-LSTM with CEBRA embeddings also outperform EEGNet with binned spikes.

Table 8.2: Model performance comparison on sequences

Input	Dimensions	Window (ms)	Model	Accuracy (%)
<b>CEBRA embeddings</b>	<b>3</b>	<b>60</b>	<b>CNN-LSTM</b>	<b>81.8</b>
Binned spikes	75	62.5	CNN-LSTM	24.8
Binned spikes	75	62.5	EEGNet	69.8

<sup>3</sup> The result visualizations were included in Appendix A.3.

Table 8.1: Model performance across different CEBRA parameters

Accuracy (%)	Offset 1			Offset 10			Offset 20		
	SVM	RF	XGBoost	SVM	RF	XGBoost	SVM	RF	XGBoost
Time	27.4	27.2	26.2	26.5	25.8	25.2	25.3	25.5	24.3
Behavior	36.2	35.7	34.6	69.2	70.4	69.8	75.3	75.7	75.2
<b>Behavior shuffled over labels</b>	36.3	35.6	34.5	<b>64.0</b>	<b>63.7</b>	<b>64.0</b>	<b>64.0</b>	<b>64.2</b>	<b>64.2</b>
Behavior shuffled over samples	25.3	25.6	24.1	24.7	25.2	23.8	26.9	27.2	26.0
Hybrid	28.0	27.7	26.2	28.9	29.3	28.2	27.0	26.9	24.6

## 8.3 Discussion

### 8.3.1 Achievements of CEBRA Embeddings

Classification results from CEBRA embeddings achieve accuracies of 64.0% and 81.8%, outperforming all previous benchmarks. CEBRA effectively squeezes the original 75 dimensions to 3, which greatly reduces the sparsity in the data. Offset 20 models consistently yield the best decoding results, possibly because the timescale of offset 20 (200 ms) captures the lengths of syllables.

The circular shape suggests that CEBRA is able to capture the syllable transitions even when trained on shuffled data. Unshuffled data contains information about syllable transitions. Training on unshuffled data achieves higher decoding accuracy of 75.7%.

### 8.3.2 Limitations

CEBRA has been validated in paradigms with clearly defined boundaries in time. Vocal productions are spontaneous and are not triggered by temporally bounded stimuli. Thus, data pre-processing is required to remove the nonactive parts in the dataset, as simply allowing the model to self-supervise over the continuous recording session leads to low efficiency and low decoding accuracy.

In addition, syllable transitions are continuous during vocalization, and pre-motor neural activity might overlap between adjacent syllables in one motif. Using data from the motor pathway would provide better results.

### 8.3.3 Future Directions

Future work could focus on contrastive learning frameworks due to their high potential to decode neural data. However, categorical labels like syllables, or redundant and high-dimensional labels like spectrograms might not be the most natural or efficient behavioural labels to use. MFCCs or latent embeddings from pre-trained models (for either human or bird vocalization) should be considered, as they are denser and have shown better performance in decoding tasks (Défossez et al., 2022b).

## Chapter 9

# Experiment 5: VAE Latent Representations

Our analysis focused on reconstructing the data using latent representations obtained from Variational Auto-Encoder (VAE). We attempted to capture patterns using both small segments as well as the whole syllable as units. We evaluated how well these generated neural latent embeddings preserve the original information through reconstruction and classification experiments.

### 9.1 Methods

The following section describes three experiments conducted. We aimed to reconstruct both neural and vocal data, investigating the correlation between paired neural and vocal data, and investigate the possibility to generate vocalization from neural data.

#### 9.1.1 Generation Experiment

We would like to investigate whether the patterns in the neural data could be captured by VAEs. In this experiment, we examined different methods to extract neural and vocal data separately to avoid encoding temporal information in the data. With the data obtained, we evaluated by visualizing the reconstructed data, investigating the latent embeddings, and training basic ML models on syllable classification tasks using

the latent embeddings of either neural or vocal data obtained from the trained models.

### 9.1.2 Correlation Experiment

For the second experiment, we applied linear warping to both neural data and spectrograms and mapped them to the maximum sequence length. With warped data, we aimed to investigate the correlation between latent embeddings generated, so that we can investigate the variance between neural and vocal data, as indicated in Singh Alvarado et al. (2021). The results of warped data were also included for reconstruction visualization, latent embedding visualization, as well as syllable classifications for completeness.

### 9.1.3 Cross-Modal Transfer: `neuro2voc`

We investigated the possibility of generating speech data with neural data. We first created a joint VAE with a speech encoder, a neural encoder, as well as a speech decoder. We trained the VAE first using only speech data to obtain a satisfactory latent representation of speech data. Then, we froze the parameters of the speech encoder, and passed in both speech and neural data together. We used contrastive learning to generate the latent embeddings of neural data to make it align with the neural data as close as possible. The result is evaluated using reconstruction visualization, latent embedding visualization, as well as syllable classification.

The quality of cross-modal transfer using a mapper function depends on not just the mapper function, but also the quality of reconstructed data in both modalities. The above method was chosen due to the unsatisfactory reconstruction quality of neural data.

## 9.2 Data Preparation

This following section describes the details of data preparation for binary neural data, binned neural data, and vocal data.

### 9.2.1 Generation Experiment: Binary Neural Data

For binary data, we selected neural data during active vocalization. We divided the activity into 30 ms segments. A moving window of step size 10 ms was used. The choice of segment length was made due to computation constraints.

### 9.2.2 Generation Experiment: Binned Neural Data

For binned data, we used three approaches to extract data: The first approach was similar to what we did to the binary neural data. We divided the data into 40 ms segments, and we used a moving window of 4 ms step size. Since some data were less than 40 ms, we padded all the data using real neighboring neural activities to increase the amount of the training data. The neural data extraction began 20 ms before each annotated syllable onset and ended earlier by the same amount.

The second approach is cutting the all the sequences according to the shortest data sequence. The smallest data sequence is 60 ms from syllable 6. However, 40 ms was first chosen to compare to the results from sliding windows above, and 80 ms were then chosen after visualizing the distribution of data, as 97.5% data are longer than or equal to 80 ms. We would like to investigate the effect of the extra 40 ms on the classification accuracy. The neural data extraction began 50 ms before each annotated syllable onset.

The third approach is padding all sequences according to the longest data with zeros. The longest sequence is 270 ms. The neural data extraction also began 50 ms before each annotated syllable onset. The padded data is excluded from discussion as it encodes temporal information. Nevertheless, the result is presented together with other types of extracting methods.

### 9.2.3 Generation Experiment: Vocal Data

For vocal data, spectrograms were provided in 128 frequency bins. The approaches were the same as the approaches for Binned Neural Data above.

The first approach was the sliding window extraction approach for binned neural data, and we made sure that neural data and vocal data are correctly aligned in content and in length through visualization.

The second approach was similar to trimming binned neural data, 40 ms was chosen in order to align with the neural data as well as the length of segments from sliding windows.

At the end, we padded all vocal data to the the maximum sequence, which was 224 ms. The neural data had a maximum sequence length of 260 ms. It was longer because (1) binning was employed on the original sample time data, (2) 50 ms were added to the original neural data before the onset. This had no effect for the generation experiment as only single modalities were used. Similar to padded neural data, the result for padded vocal data is excluded from textual discussion, but the visualizations were presented in the result section as well for completeness.

### 9.2.4 Correlation Experiment: Neural and Vocal Data

We first normalized the time to 0–1, and we created interpolation function for individual frequency bin. Then we sample at new time points. The vocal data were warped to a maximum sequence of length 224 ms. Neural data were warped similarly to a maximum sequence of length 260 ms.

### 9.2.5 Cross-Modal Transfer: Neural and Vocal Data

For cross-modal transfer, we used segmented neural and vocal data on three levels: 4 ms, 40 ms, and 80 ms. Both data were extracted such that they are aligned in sequence length. The neural data were binned with a window size of 4 ms to match the sampling frequency of vocal data (250 Hz).

## 9.3 Models and Evaluation

The data were passed to the following models:

1. 1D VAE: a VAE composed of Conv1D layers for neural data
2. 2D VAE: a VAE composed Conv2D layers for vocal data, based on Singh Alvarado et al. (2021)

3. NeuralEnCodec: a VAE aiming at lossless reconstruction of neural data, based on EnCodec of Défossez et al. (2022b)
4. Joint VAE: a VAE composed of Conv1D for neural data and Conv2D for vocal data

We first briefly describe the training progress through the observation of the reconstruction loss, Mean Squared Error (MSE). Then we included in the results section a simple visualization of the final reconstructed data using random data on the test set (an 8/2 split was used).

After the models were trained, all data were combined and passed again into the encoder to obtain the latent representations. The latent representations (which were 32-dimensional) of all data were visualized in 2D using Uniform Manifold Approximation and Projection (UMAP) and color-coded with syllable types. The latent representations were also passed to SVM, RF, and XGBoost for syllable classification tasks. The classification accuracies of neural data were compared to CEBRA under the same conditions.

The warped neural and vocal latent representations were used to perform a Canonical Correlation Analysis. The first few Canonical Components were visualized and we reported the correlation coefficient.

## 9.4 Visualization Results

### 9.4.1 Generation Experiment: Visualization<sup>4</sup>

In all experiments, all the neural models showed convergence early and the loss were high, suggesting more training data would be needed. Since 2D VAE and NeuralEnCodec repeatedly showed insatisfactory reconstruction results on binary and warped neural data, they were not used for further analysis in generation experiments for neural data. Some reconstruction visualizations were included in the results section for completeness, but only 1D VAE was used for neural data for further processing as well as detailed evaluation.

---

<sup>4</sup> All the neurons used in the visualization in this experiment were ranked by the depth to the tip, where N0 is the closest to the probe tip.

### 9.4.1.1 Binary Neural Data - Segments of 30 ms

1D VAE showed little amount of learning and produced poor reconstruction quality. Figure 9.1 shows the original and the reconstructed binary neural data. Different scales are used for the reconstructed neural data, because the results are visually imperceptible in the reconstructed data using the original scale.

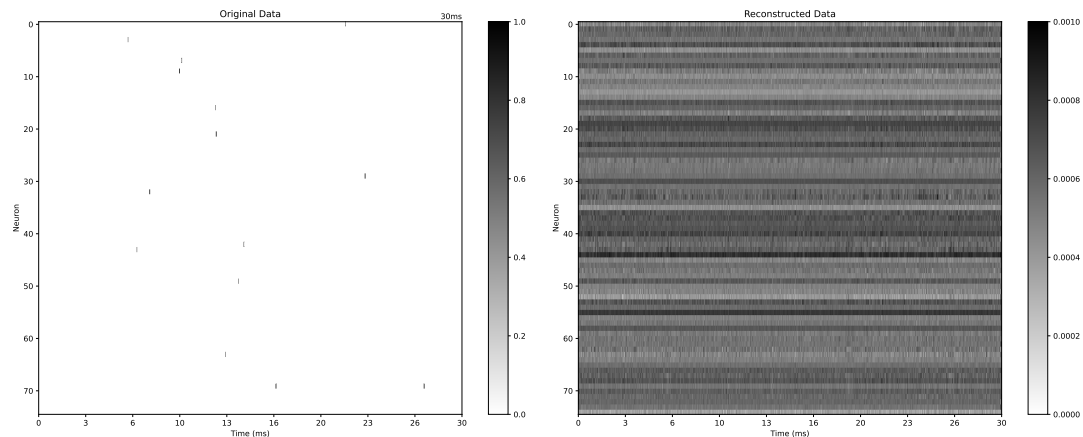


Figure 9.1: Reconstruction of binary neural data – 1D VAE

NeuralEnCodec reached the best result early, and showed limited learning progress. The reconstruction in Figure 9.2 shows temporal smoothing patterns. Instead of reproducing the precise spikes, the model generates an averaged spiking pattern across time. Similarly, different scaled were used in the figure, because the results were visually imperceptible in the reconstructed data using identical scales.

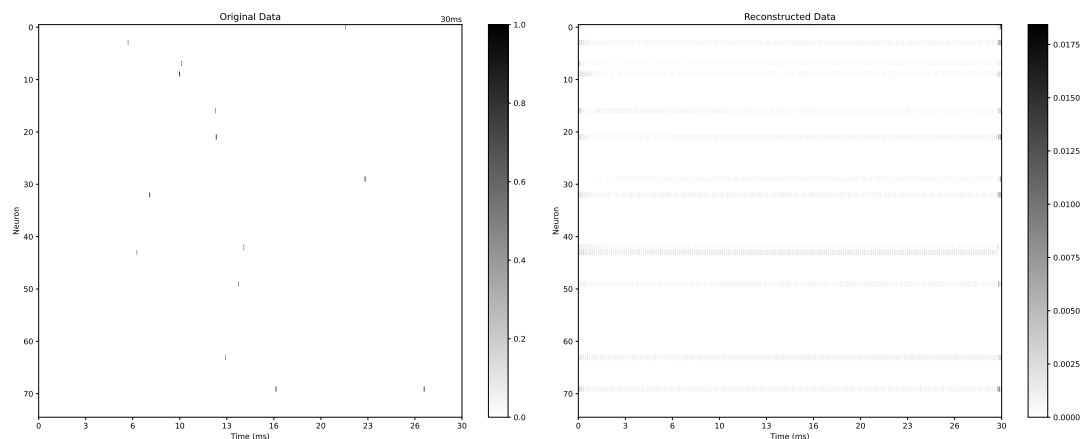


Figure 9.2: Reconstruction of binary neural data – NeuralEnCodec

### 9.4.1.2 Binned Neural Data - Segments of 40 ms

Figure 9.3 shows the reconstruction results of 1D VAE trained on binned neural data. The results were not good enough, and some basic patterns in the original data were not captured. A binning window of 4 ms was used.

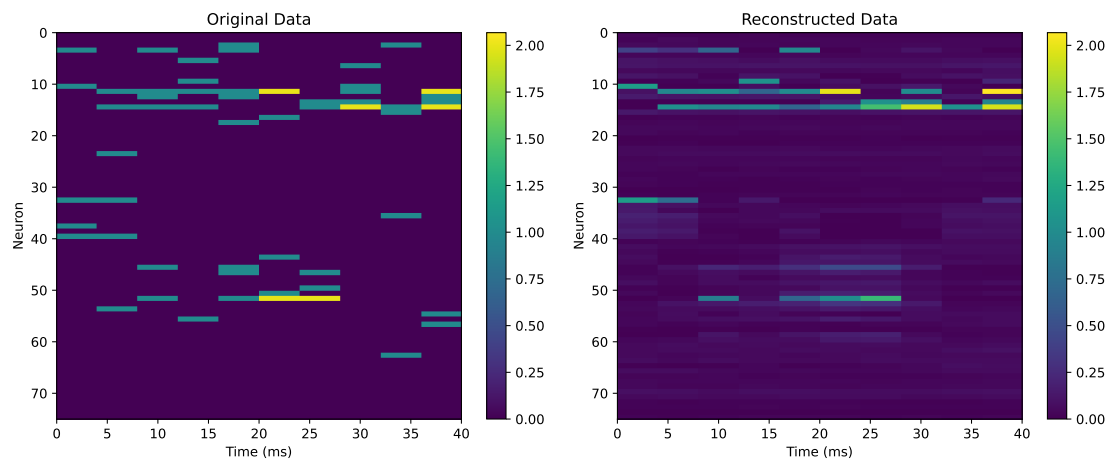


Figure 9.3: Reconstruction of binned neural data – segments of 40 ms

### 9.4.1.3 Binned Neural Data - Trimmed to 40 ms and 80 ms

Figure 9.4 and Figure 9.5 show the reconstruction results using trimmed neural activities at syllable onsets using 1D. The binning window is 10 ms.

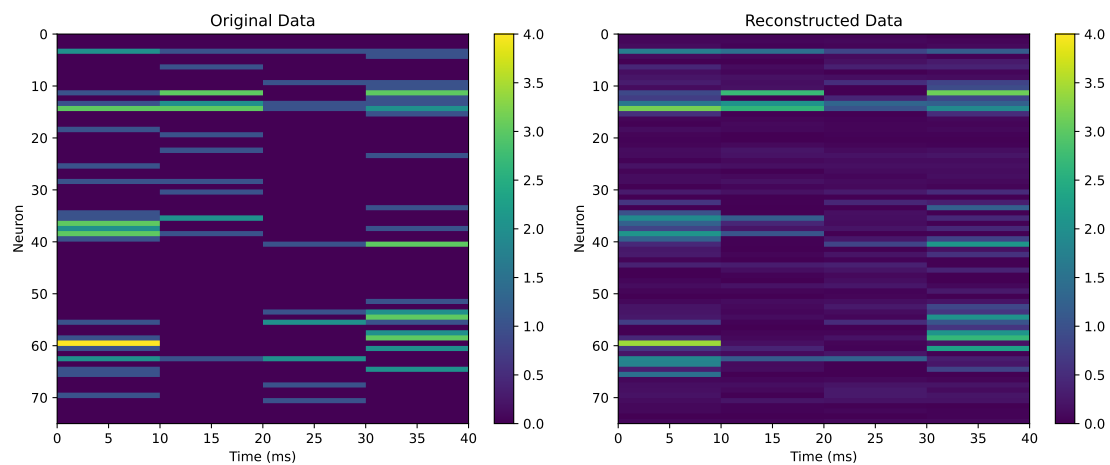


Figure 9.4: Reconstruction of binned neural data – trimmed to 40 ms

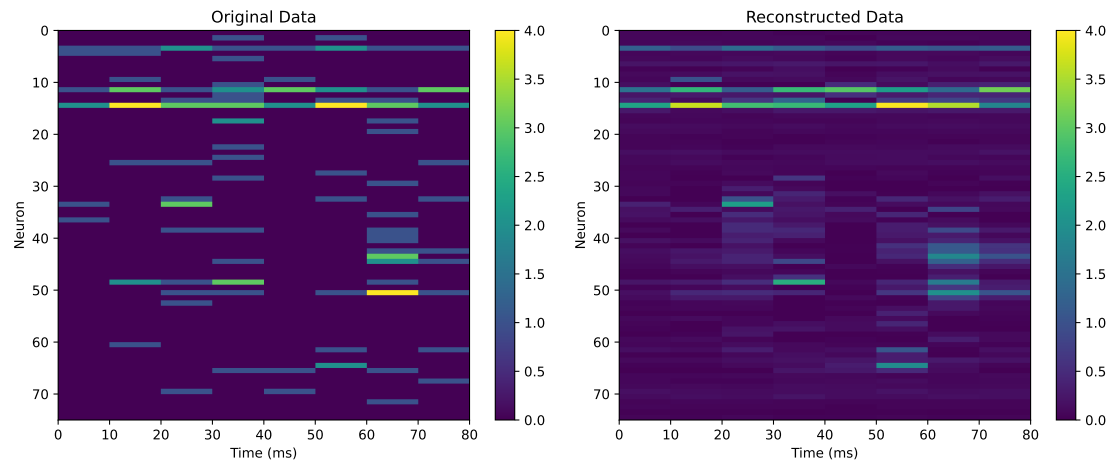


Figure 9.5: Reconstruction of binned neural data – trimmed to 80 ms

#### 9.4.1.4 Binned Neural Data - Padded to 270 ms

Figure 9.6 shows the reconstruction results using 1D VAE. Each neural data is padded to the maximum sequence length. Data were binned using a 10 ms window.

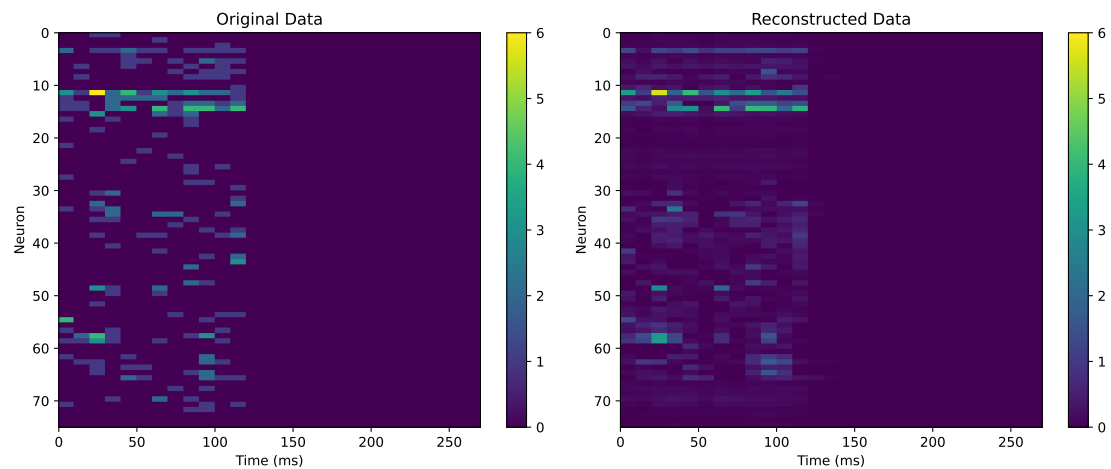


Figure 9.6: Reconstruction of binned neural data – padded to 270 ms

### 9.4.1.5 Vocal Data - Segments of 40 ms

Figure 9.7 shows the reconstruction results for 10 random vocalization segments using 2D VAE. Each segment is extracted from sliding windows and lasts for 40 ms.

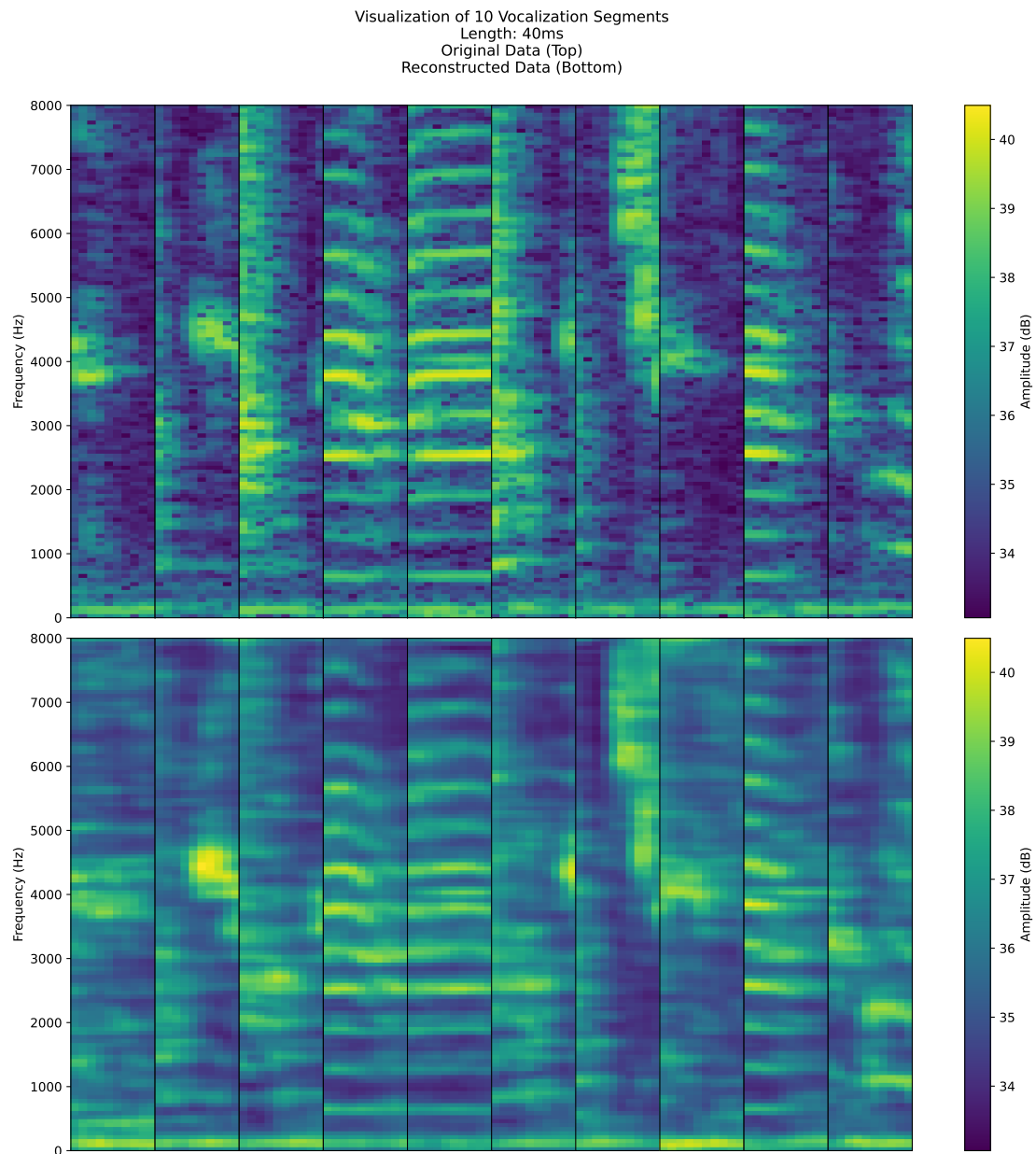


Figure 9.7: Reconstruction of segmented vocal data – segments of 40 ms

### 9.4.1.6 Vocal Data - Trimmed to 40 ms

Figure 9.8 shows the reconstruction results from 2D VAE of random vocalization syllables using 2D VAE, from 2 to 8. Only the first 40 ms was kept for each annotated syllable.

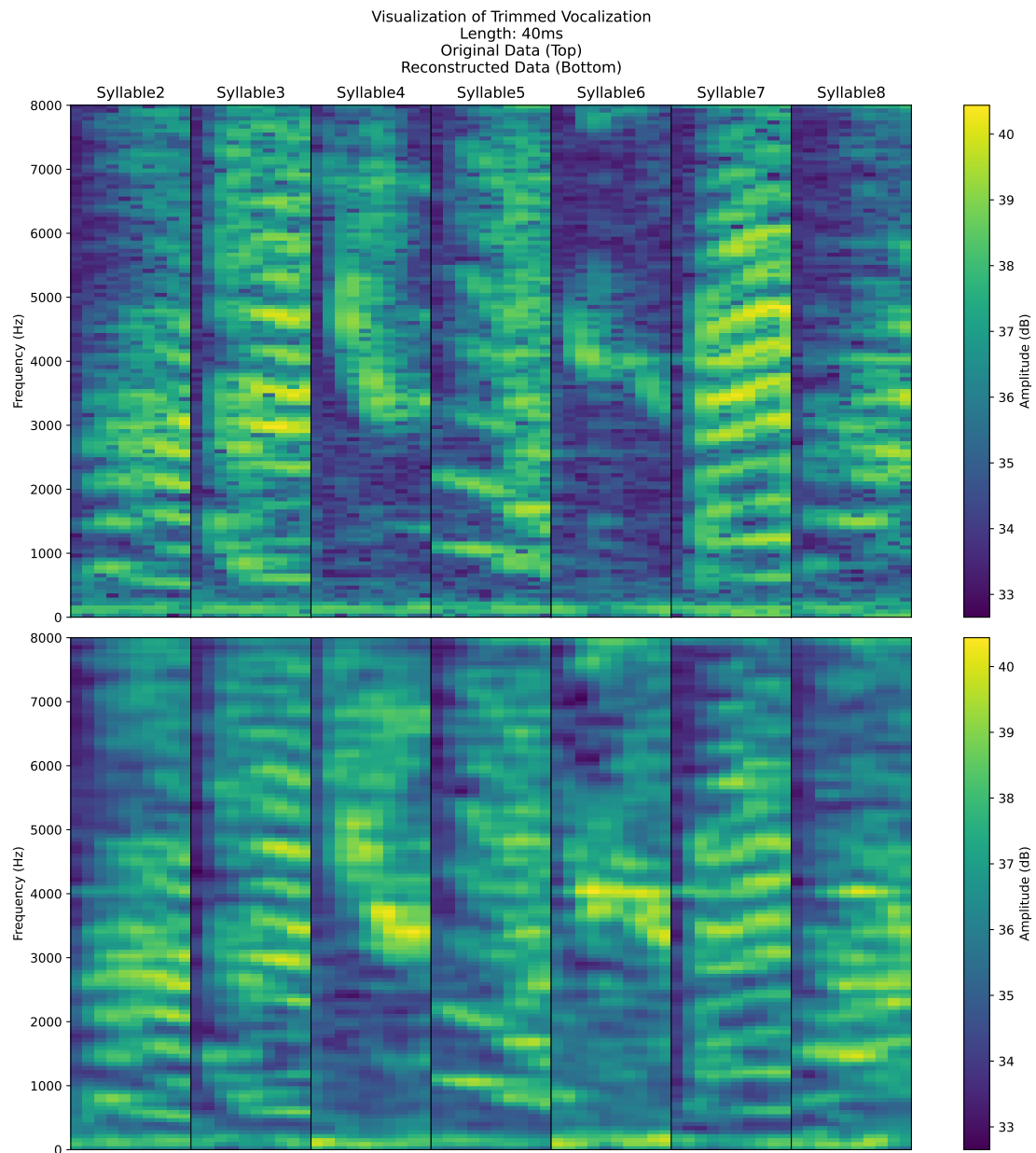


Figure 9.8: Reconstruction of trimmed vocal data – trimmed to 40 ms

### 9.4.1.7 Vocal Data - Padded to 224 ms

Figure 9.9 shows the reconstruction results from 2D VAE of random vocalization syllables. Each syllable was padding to 224 ms.

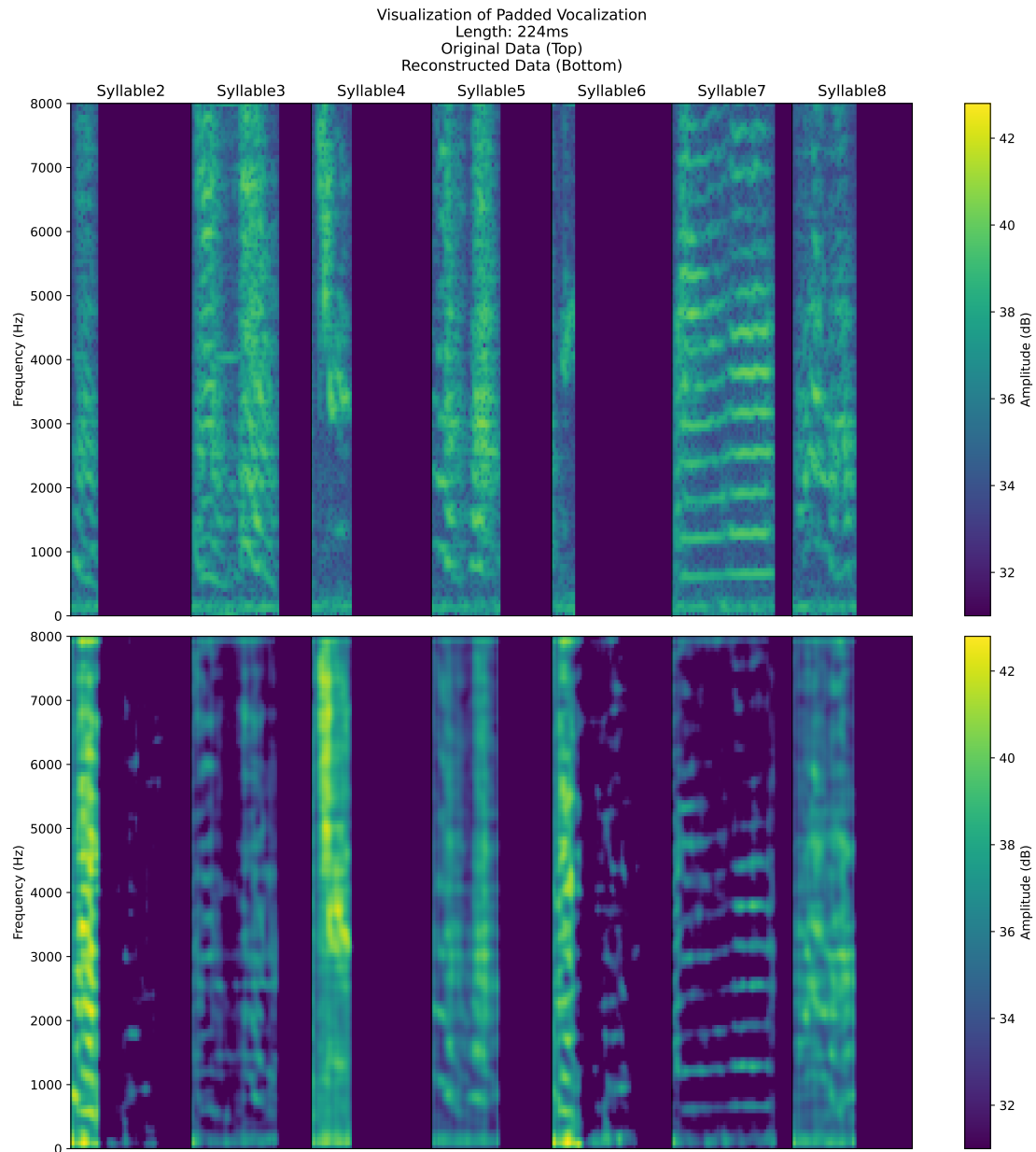


Figure 9.9: Reconstruction of padded vocal data – padded to 224 ms

## 9.4.2 Correlation Experiment: Visualization

### 9.4.2.1 Binned Neural Data - Warped

The reconstruction loss from 1D VAE was consistently decreasing. Figure 9.10 showed the original neural data on the left, and the reconstructed neural data on the right from 1D VAE. Neural data showed satisfactory reconstruction results upon visual inspection.

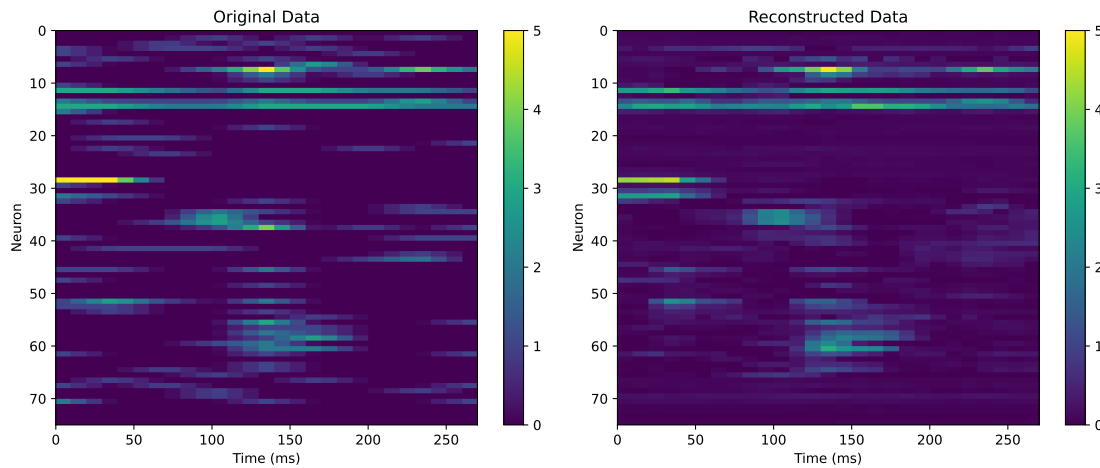


Figure 9.10: Reconstruction of warped and binned neural data with 1D VAE

NeuralEnCodec reached the best result as early as Epoch 12. The result is shown below. Similarly to its performance on binary data shown in Figure 9.2, NeuralEnCodec captured some characteristics of data, but smoothed out the data over time.

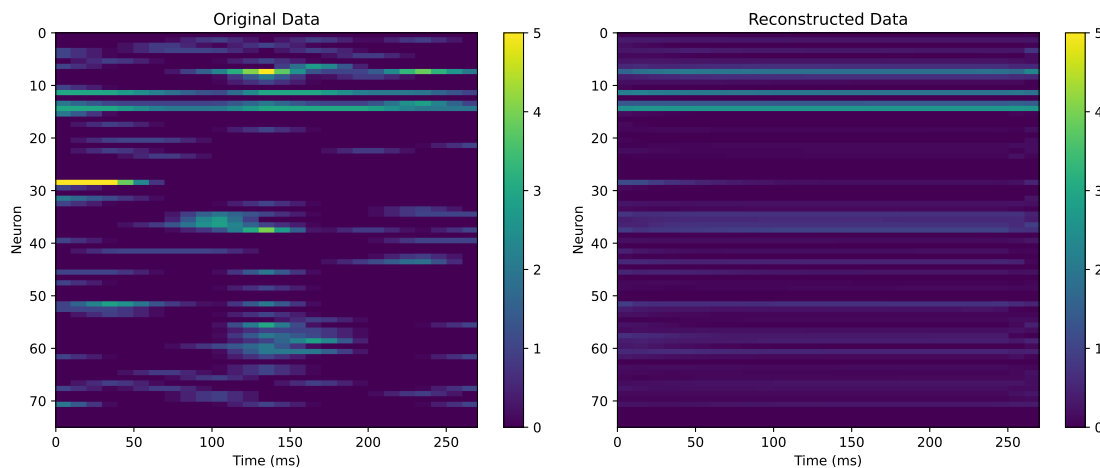


Figure 9.11: Reconstruction of binary neural data with NeuralEnCodec

### 9.4.2.2 Vocal Data - Warped

Figure 9.12 shows original and reconstructed data for all different syllables using 2D VAE. The visualization was averaged over all warped samples. <sup>5</sup>

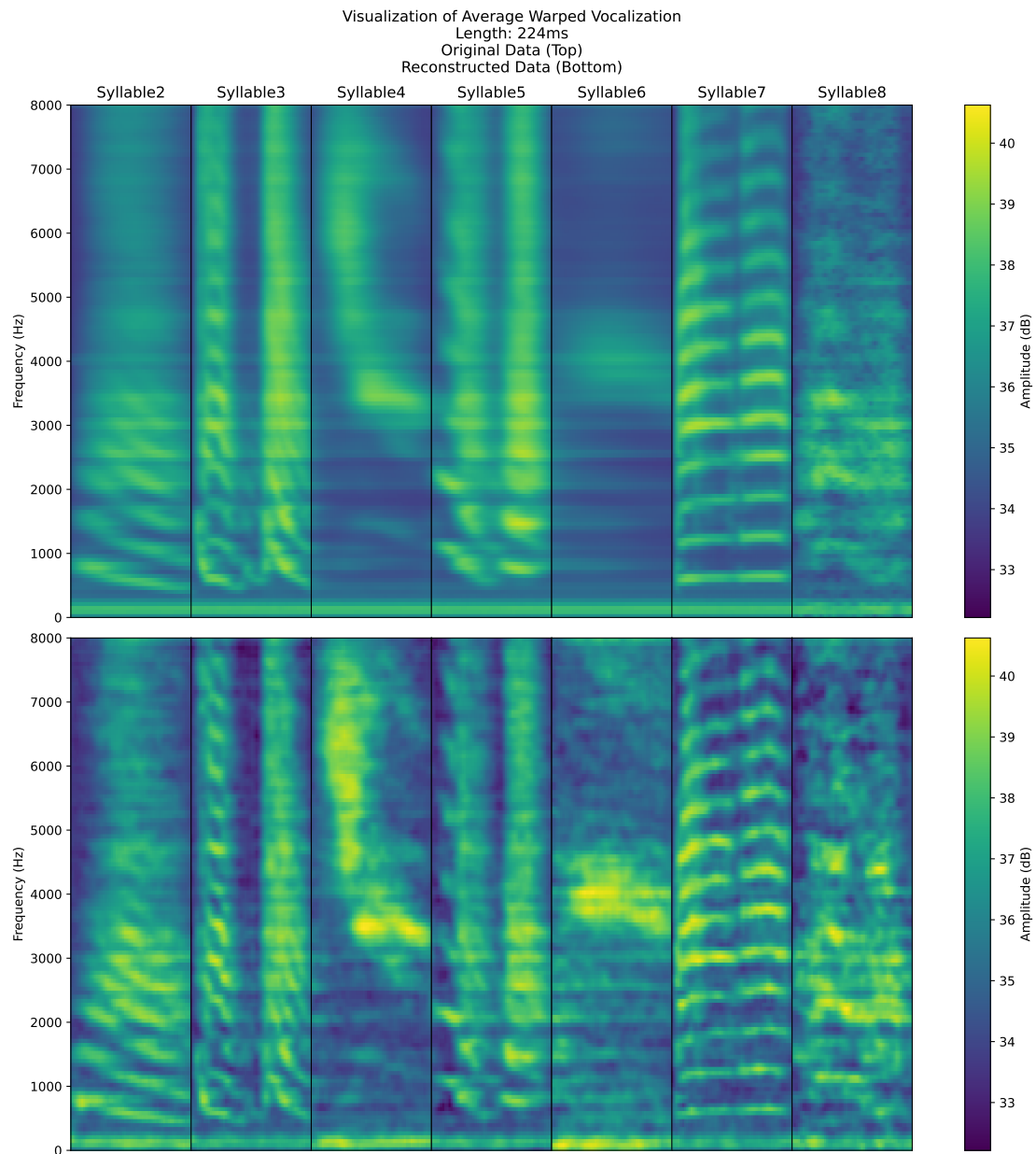


Figure 9.12: Reconstruction of warped vocal data

<sup>5</sup> Individual visualizations of averaged data and random samples are included in Appendix A.4

### 9.4.3 Cross-Modal Transfer: neuro2voc

Figure 9.13 shows the generated vocal data from neural data inputs. The neural data were obtained with sliding windows with 40 ms<sup>6</sup> sequence length.

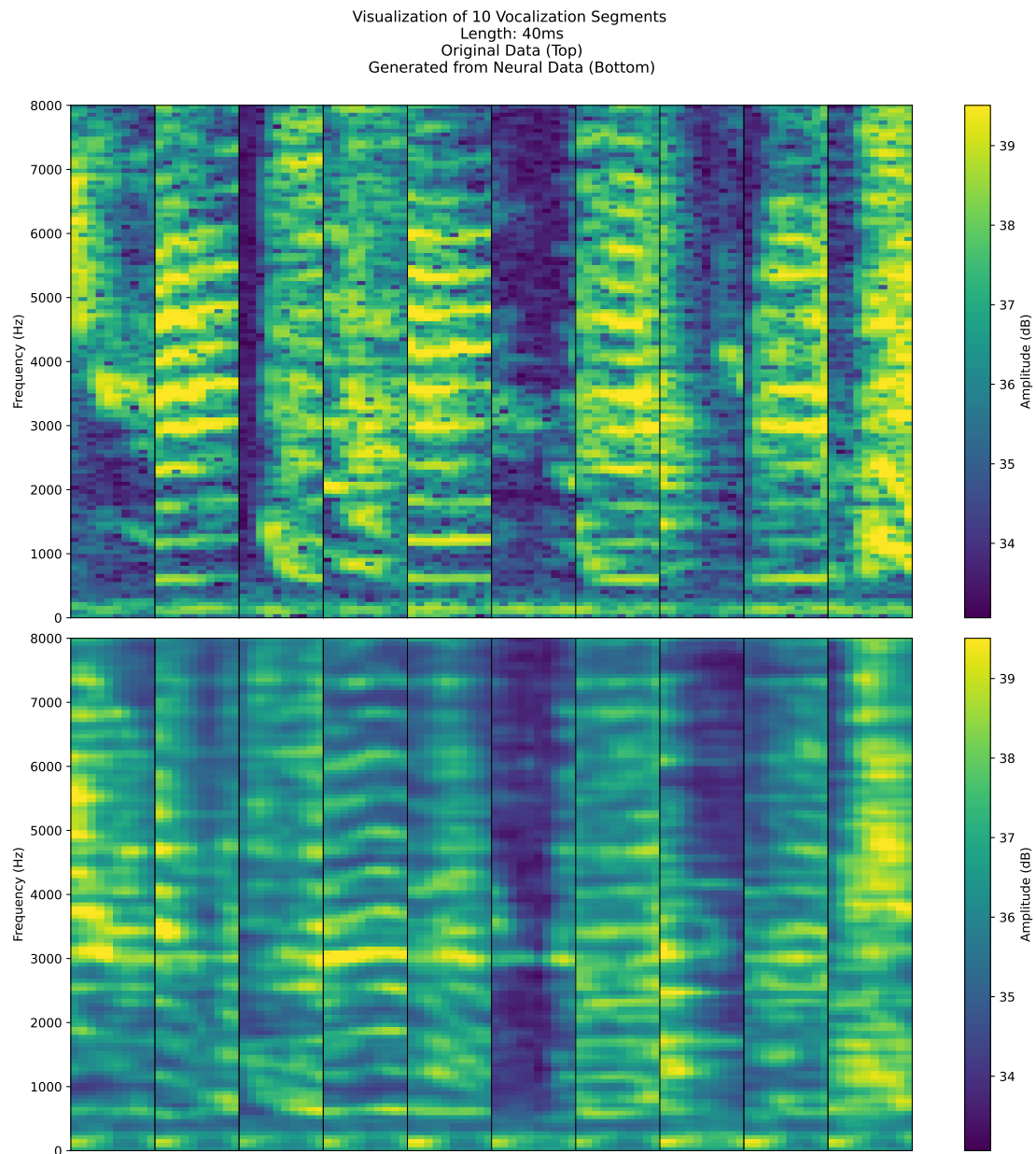


Figure 9.13: Generate 40 ms vocalization from 40 ms neural data

<sup>6</sup> Visualization for 80 ms is included in Appendix A.4

## 9.5 Latent Representation Evaluations

### 9.5.1 Visualization of Latent Representations

Figure 9.14 shows the UMAP projection of latent representations obtained from the generation experiment. Figure 9.15 shows the result from the cross-modal transfer experiment. The neural representations only showed clustering effect after aligning to pre-trained vocal representations through contrastive learning.

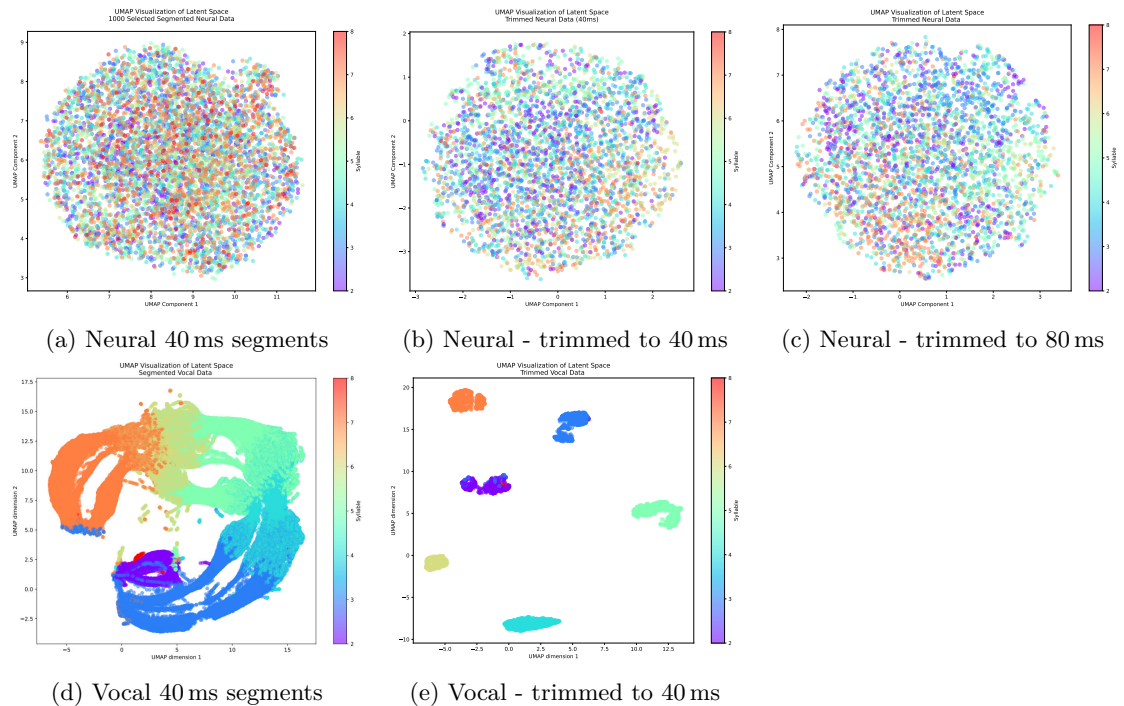


Figure 9.14: UMAP visualization of latent representations from generation experiment

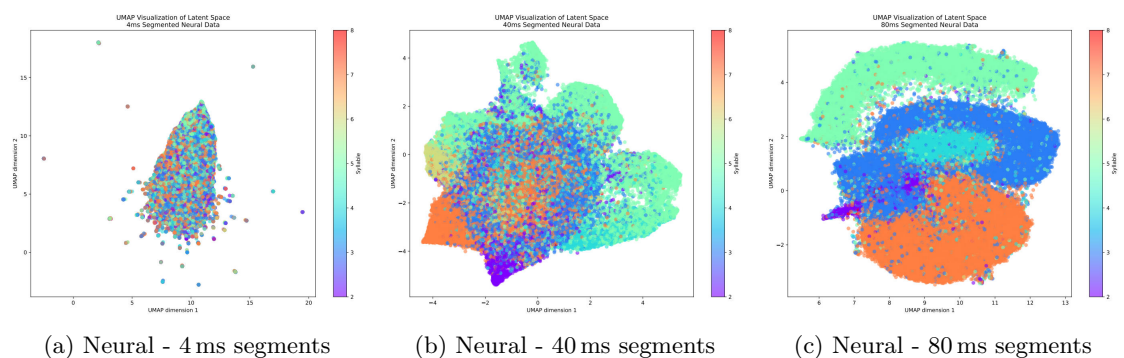


Figure 9.15: UMAP visualization of latent representations from neuro2voc experiment

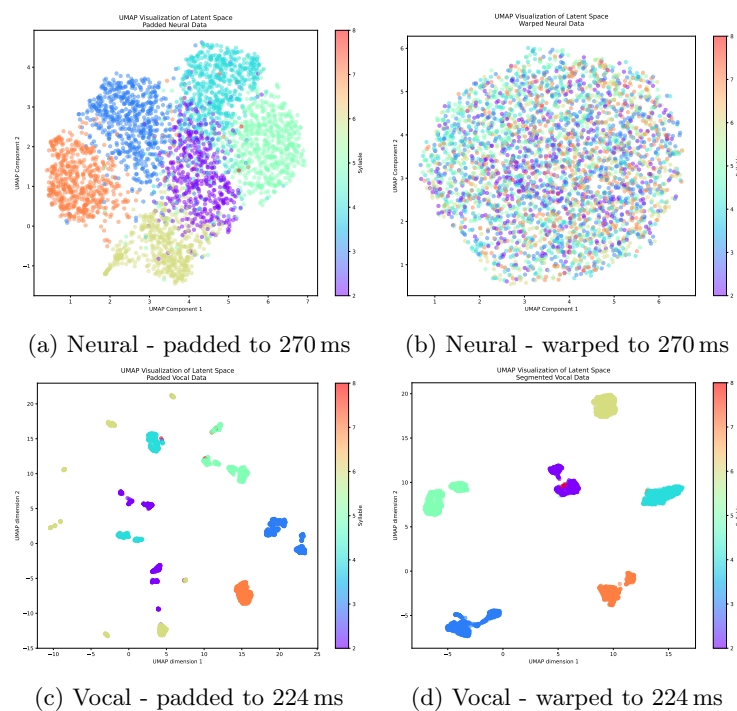


Figure 9.16: UMAP visualization of latent representations from correlation experiment

Figure 9.16 shows clear patterns of clustering in both vocal representations and neural representations, due to encoded temporal information during warping.

## 9.5.2 Classification with Latent Representations

The latent representations of both neural and vocal data were used to perform syllable classification tasks. From Table 9.1, the vocal data achieved high decoding accuracy, and thus conveyed the syllable information better.

For the neural data, the padded and warped data in light gray have highest performance but encode temporal information. Trimmed neural data of length 40 ms, obtained at period  $[-50 \text{ ms}, -10 \text{ ms}]$ , achieved an accuracy of 49.9% with SVM. This is better than the 27.7% accuracy segmented neural data of the same length, which were obtained using sliding windows. The decoding efficiency of segmented neural data improved to 72.5% after using contrastive learning to align with pre-trained vocal data.

Table 9.1: Syllable classification accuracies (%)

Data	Experiment	Method	Window (ms)	Duration (ms)	SVM	RF	XGBoost
Neural Data	Generation	Segmented	4	40	27.7	25.8	26.8
	Generation	Trimmed	10	40	49.9	45.5	48.1
	Generation	Trimmed	10	80	53.5	45.2	50.1
	Generation	Padded	10	270	96.4	93.5	93.5
	Correlation	Warped	10	270	75.6	63.6	67.8
	Contrastive	Segmented	4	4	35.1	32.4	34.1
	<b>Contrastive</b>	<b>Segmented</b>	<b>4</b>	<b>40</b>	<b>72.5</b>	<b>65.2</b>	<b>69.3</b>
	<b>Contrastive</b>	<b>Segmented</b>	<b>4</b>	<b>80</b>	<b>91.0</b>	<b>84.4</b>	<b>89.6</b>
Vocal Data	Generation	Segmented	4	40	79.7	68.5	73.1
	Generation	Trimmed	4	40	98.8	98.0	97.8
	Correlation	Padded	4	224	96.4	93.5	93.5
	Correlation	Warped	4	224	99.4	99.3	98.8

## 9.6 Canonical Component Analysis

Figure 9.17 shows that the first two pairs of Canonical Components are strongly correlated ( $R > 0.6$ ). This indicates that the variations among neural data is correlated with the variations among vocal data.

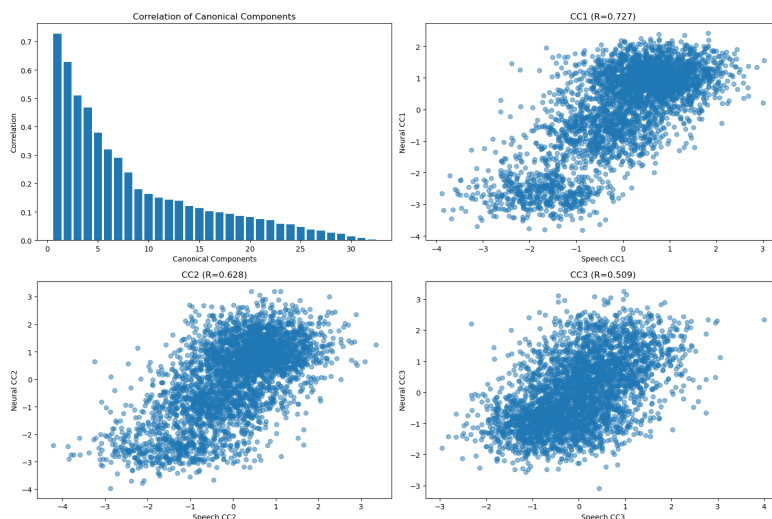


Figure 9.17: Result from canonical component analysis

## 9.7 Discussion

### 9.7.1 Achievements of Latent Representations from VAE

We showed different ways to process and reconstruct vocal and neural data, as well as the corresponding qualities of reconstruction. With the models and data from this project, the reconstruction quality was high for all vocal data and warped neural data, and the quality was acceptable for neural data in some modalities.

In the neuro2voc experiment, we combined contrastive learning with generative models, and successfully reconstructed vocal data using neural data. After contrastive learning methods, the decoding accuracy of segmented 40 ms data were enhanced from 27.7% to 72.5%. The highest decoding accuracy was 91.0% from neural data of length 80 ms, where the data segments were obtained with a sliding window.

### 9.7.2 Limitations

During training, the models showed different patterns for vocal and neural data. Training on vocal data exhibited clear learning progress in terms of loss reduction. In contrast, training on neural data models reached plateaux very early. This indicates two things that are essential for better reconstruction of neural data: (1) more training data, and (2) a more sophisticated VAE structure.

### 9.7.3 Future Directions

A larger dataset of neural recordings is essential to enhance the model performance. We also observed that the 1D architecture performed better than the 2D model on neural data during training. The 2D VAE successfully captured relationships in spectrograms. However, it failed to detect connections among neuron populations. As EEGNet showed high decoding accuracy in Experiment 3, its structure could also be integrated into current VAE structure. These observations point to a clear direction for VAE on binned spike data.

# Chapter 10

## Conclusion

### 10.1 Achievements

This project establishes several pilot frameworks in neural decoding and analysis.

#### 10.1.1 Neural Activity Analysis and Classification

We created a classification baseline using mean firing rates, achieving 77.3% accuracy with SVM for syllable classification tasks. We combined XGBoost and SHAP analysis to reveal syllable-specific firing patterns and important neuron interactions. We also identified temporal relationships between LMAN burst and syllable production from the output of basic machine learning models, which aligns with neuroscience literature.

#### 10.1.2 Decoding Frameworks with New Architectures

We developed a new framework to decode spike data, and demonstrated the potential of GPT-2 for neural decoding. We also investigated the decoding accuracy of simpler models using LSTM, CNN, Mamba-2, etc. EEGNet achieved the highest decoding accuracy (89.0%). Mamba2 showed better performance when the data is sparse and long. We investigated the correlation of plateau point bin size of 1.5 ms with the scale of AP.

### 10.1.3 Generative Model with Contrastive Learning

We implemented 15 models in CEBRA and achieved an accuracy as high as 75.7% on syllable classification tasks. We confirmed the advantage that a contrastive learning framework offers. We also investigated the potential of VAE on all types of processed neural and vocal: segmented, trimmed, padded, warped, and in different durations.

We used a combined contrastive-generative approach, achieving 91.0% accuracy on syllable classification. The model offers the possibility to generate segmented vocal data from segmented neural data. In addition, CCA revealed strong correlations ( $r = 0.73$ ) between warped neural and vocal representations.

## 10.2 Limitations

This project had several limitations.

### 10.2.1 Data Dependency and Generalization Challenges

The decoding framework's reliance on annotated syllables creates a circular dependency, which limits the practical applications. The performance of the models on different birds was untested, and the transferability between different birds may be highly limited, as different birds have distinct syllables.

### 10.2.2 Data Volume Constraints

The data is insufficient for the current models to converge. A larger dataset would yield higher decoding accuracy of syllables or better reconstruction quality of neural data.

### 10.2.3 Biological Plausibility

The data came from the LMAN region, which primarily controls plasticity rather than production. Data from nuclei along the motor pathway would yield more accurate and interpretable results for decoding tasks.

## 10.3 Future Direction

The project establishes methodological foundations for future research, emphasizing the balance between computational performance, model interpretability, and biological plausibility through its achievements and limitations.

### 10.3.1 Syllable-Based Approaches

With data recorded from the motor pathway, the SHAP interaction values can be used to visualize how neurons integrate information and control the output syllables.

Depending on the availability of data, a pre-trained model based on open source models like GPT-2 on multiple birds and syllables could be developed. With a pre-trained model, latent embeddings could serve as a target of interpretability analysis.

Mamba2 showed potential for decoding long and sparse spike trains. EEGNet and Mamba2 can be further investigated and developed in this direction to decode spike data in 20 kHz or 30 kHz with higher accuracies.

### 10.3.2 Representation Learning

Decoding neural activities with the CEBRA method using pretrained latent embeddings (like wav2vec) would improve interpretability on a finer scale. The CEBRA method could also be combined into the current joint VAE to better align neural representations to vocal representations in VAE. VAE framework itself could be further improved with statistical inference methods to better capture the patterns in the neural data.

### 10.3.3 NeuroAI

Recent advances in neuroscience and AI have given rise to a new field known as NeuroAI (Benchetrit et al., 2023; Conwell et al., 2023; Francl and McDermott, 2022; Yamins et al., 2014; Yamins and DiCarlo, 2016). While current NeuroAI research focused primarily on visual perception, our project suggest promising direction of extending the work of NeuroAI to motor vocalization. Generative models can be built with song circuit inspired neural network architectures, while simultaneous recordings from the motor pathway

and AFP could be used as inputs. Future work can perform ablation studies on layers representing LMAN, and evaluate the neural network by observing the variability in the reconstructed syllable.

# References

- Aaron S Andalman and Michale S Fee. 2009. A basal ganglia-forebrain circuit in the songbird biases motor output to avoid vocal errors. *Proc. Natl. Acad. Sci. U. S. A.*, 106(30):12518–12523.
- Mehdi Azabou, Vinam Arora, Venkataramana Ganesh, Ximeng Mao, Santosh Nachimuthu, Michael J Mendelson, Blake Richards, Matthew G Perich, Guillaume Lajoie, and Eva L Dyer. 2023. A unified, scalable framework for neural population decoding. *arXiv [cs.LG]*.
- Alexei Baevski, Henry Zhou, Abdelrahman Mohamed, and Michael Auli. 2020. Wav2vec 2.0: A framework for self-supervised learning of speech representations. *arXiv [cs.CL]*.
- Yohann Benchetrit, Hubert Banville, and Jean-Rémi King. 2023. Brain decoding: toward real-time reconstruction of visual perception. *arXiv [eess.IV]*.
- Bernhard E Boser, Isabelle M Guyon, and Vladimir N Vapnik. 1992. A training algorithm for optimal margin classifiers. In *Proceedings of the fifth annual workshop on Computational learning theory*, New York, NY, USA. ACM.
- S W Bottjer, E A Miesner, and A P Arnold. 1984. Forebrain lesions disrupt development but not maintenance of song in passerine birds. *Science*, 224(4651):901–903.
- Rewon Child, Scott Gray, Alec Radford, and Ilya Sutskever. 2019. Generating long sequences with sparse transformers. *arXiv [cs.LG]*.
- Srikanta Chowdhury, Takanori Matsubara, Toh Miyazaki, Daisuke Ono, Noriaki Fukatsu, Manabu Abe, Kenji Sakimura, Yuki Sudo, and Akihiro Yamanaka. 2019.

GABA neurons in the ventral tegmental area regulate non-rapid eye movement sleep in mice. *eLife*, 8.

Colin Conwell, Jacob S Prince, Kendrick N Kay, George A Alvarez, and Talia Konkle. 2023. What can 1.8 billion regressions tell us about the pressures shaping high-level visual representation in brains and machines? *bioRxiv*, page 2022.03.28.485868.

Tri Dao and Albert Gu. 2024. Transformers are SSMs: Generalized models and efficient algorithms through structured state space duality. *arXiv [cs.LG]*.

Saskia E J de Vries, Jerome A Lecoq, Michael A Buice, Peter A Groblewski, Gabriel K Ocker, Michael Oliver, David Feng, Nicholas Cain, Peter Ledochowitsch, Daniel Millman, Kate Roll, Marina Garrett, Tom Keenan, Leonard Kuan, Stefan Mihalas, Shawn Olsen, Carol Thompson, Wayne Wakeman, Jack Waters, Derric Williams, Chris Barber, Nathan Berbesque, Brandon Blanchard, Nicholas Bowles, Shiella D Caldejon, Linzy Casal, Andrew Cho, Sissy Cross, Chinh Dang, Tim Dolbeare, Melise Edwards, John Galbraith, Nathalie Gaudreault, Terri L Gilbert, Fiona Griffin, Perry Hargrave, Robert Howard, Lawrence Huang, Sean Jewell, Nika Keller, Ulf Knoblich, Josh D Larkin, Rachael Larsen, Chris Lau, Eric Lee, Felix Lee, Arielle Leon, Lu Li, Fuhui Long, Jennifer Luviano, Kyla Mace, Thuyanh Nguyen, Jed Perkins, Miranda Robertson, Sam Seid, Eric Shea-Brown, Jianghong Shi, Nathan Sjoquist, Cliff Slaughterbeck, David Sullivan, Ryan Valenza, Casey White, Ali Williford, Daniela M Witten, Jun Zhuang, Hongkui Zeng, Colin Farrell, Lydia Ng, Amy Bernard, John W Phillips, R Clay Reid, and Christof Koch. 2020. A large-scale standardized physiological survey reveals functional organization of the mouse visual cortex. *Nat. Neurosci.*, 23(1):138–151.

A J Doupe and P K Kuhl. 1999. Birdsong and human speech: common themes and mechanisms. *Annu. Rev. Neurosci.*, 22(1):567–631.

Allison J Doupe, David J Perkel, Anton Reiner, and Edward A Stern. 2005. Birdbrains could teach basal ganglia research a new song. *Trends Neurosci.*, 28(7):353–363.

Alexandre Défossez, C Caucheteux, J Rapin, Ori Kabeli, and J King. 2022a. Decoding speech perception from non-invasive brain recordings. *Nat. Mach. Intell.*, 5:1097–1107.

Alexandre Défossez, Jade Copet, Gabriel Synnaeve, and Yossi Adi. 2022b. High fidelity neural audio compression. *arXiv [eess.AS]*.

- Mirko Farina, Usman Ahmad, Ahmad Taha, Hussein Younes, Yusuf Mesbah, Xiao Yu, and Witold Pedrycz. 2024. Sparsity in transformers: A systematic literature review. *Neurocomputing*, 582(127468):127468.
- Andrew Francel and Josh H McDermott. 2022. Deep neural network models of sound localization reveal how perception is adapted to real-world environments. *Nat Hum Behav*, 6(1):111–133.
- Samuel D Gale and David J Perkel. 2010. Anatomy of a songbird basal ganglia circuit essential for vocal learning and plasticity. *J. Chem. Neuroanat.*, 39(2):124–131.
- Nicolas Giret, Joergen Kornfeld, Surya Ganguli, and Richard H R Hahnloser. 2014. Evidence for a causal inverse model in an avian cortico-basal ganglia circuit. *Proc. Natl. Acad. Sci. U. S. A.*, 111(16):6063–6068.
- Rabia Gondur, Usama Bin Sikandar, Evan Schaffer, Mikio Christian Aoi, and Stephen L Keeley. 2023. Multi-modal gaussian process variational autoencoders for neural and behavioral data. *arXiv [cs.LG]*.
- Adam Gosztolai, Robert L Peach, Alexis Arnaudon, Mauricio Barahona, and Pierre Vanderghelynst. 2023. Interpretable statistical representations of neural population dynamics and geometry. *arXiv [cs.LG]*.
- Andres D Grosmark and György Buzsáki. 2016. Diversity in neural firing dynamics supports both rigid and learned hippocampal sequences. *Science*, 351(6280):1440–1443.
- Albert Gu and Tri Dao. 2023. Mamba: Linear-time sequence modeling with selective state spaces. *arXiv [cs.LG]*.
- Laura Gwilliams, Jean-Remi King, Alec Marantz, and David Poeppel. 2022. Neural dynamics of phoneme sequences reveal position-invariant code for content and order. *Nat. Commun.*, 13(1):6606.
- Liwei Huang, Zhengyu Ma, Liutao Yu, Huihui Zhou, and Yonghong Tian. 2024. Time-dependent VAE for building latent representations from visual neural activity with complex dynamics. *arXiv [cs.NE]*.
- James J Jun, Nicholas A Steinmetz, Joshua H Siegle, Daniel J Denman, Marius Bauza, Brian Barbarits, Albert K Lee, Costas A Anastassiou, Alexandru Andrei, Çağatay Aydın, Mladen Barbic, Timothy J Blanche, Vincent Bonin, João Couto, Barundeb

- Dutta, Sergey L Gratiy, Diego A Gutnisky, Michael Häusser, Bill Karsh, Peter Ledochowitsch, Carolina Mora Lopez, Catalin Mitelut, Silke Musa, Michael Okun, Marius Pachitariu, Jan Putzeys, P Dylan Rich, Cyrille Rossant, Wei-Lung Sun, Karel Svoboda, Matteo Carandini, Kenneth D Harris, Christof Koch, John O’Keefe, and Timothy D Harris. 2017. Fully integrated silicon probes for high-density recording of neural activity. *Nature*, 551(7679):232–236.
- Mimi H Kao, Allison J Doupe, and Michael S Brainard. 2005. Contributions of an avian basal ganglia-forebrain circuit to real-time modulation of song. *Nature*, 433(7026):638–643.
- Diederik P Kingma and Max Welling. 2013. Auto-encoding variational bayes. *arXiv [stat.ML]*.
- Diederik P Kingma and Max Welling. 2019. An introduction to variational autoencoders. *arXiv [cs.LG]*.
- Satoshi Kojima, Mimi H Kao, Allison J Doupe, and Michael S Brainard. 2018. The avian basal ganglia are a source of rapid behavioral variation that enables vocal motor exploration. *J. Neurosci.*, 38(45):9635–9647.
- Alex Labach, Aslesha Pokhrel, Xiao Shi Huang, Saba Zuberi, Seung Eun Yi, Maksims Volkovs, Tomi Poutanen, and Rahul G Krishnan. 2023. DuETT: Dual event time transformer for electronic health records. *arXiv [cs.LG]*, pages 403–422.
- Vernon J Lawhern, Amelia J Solon, Nicholas R Waytowich, Stephen M Gordon, Chou P Hung, and Brent J Lance. 2016. EEGNet: A compact convolutional network for EEG-based brain-computer interfaces. *arXiv [cs.LG]*.
- Yikuan Li, Mohammad Mamouei, Gholamreza Salimi-Khorshidi, Shishir Rao, Abdelaali Hassaine, Dexter Canoy, Thomas Lukasiewicz, and Kazem Rahimi. 2023. Hi-BEHRT: Hierarchical transformer-based model for accurate prediction of clinical events using multimodal longitudinal electronic health records. *IEEE J. Biomed. Health Inform.*, 27(2):1106–1117.
- Opher Lieber, Barak Lenz, Hofit Bata, Gal Cohen, Jhonathan Osin, Itay Dalmedigos, Erez Safahi, Shaked Meïrom, Yonatan Belinkov, Shai Shalev-Shwartz, Omri Abend, Raz Alon, Tomer Asida, Amir Bergman, Roman Glozman, Michael Gokhman, Avashalom Manevich, Nir Ratner, Noam Rozen, Erez Shwartz, Mor Zusman, and

- Yoav Shoham. 2024. Jamba: A hybrid transformer-mamba language model. *arXiv [cs.CL]*.
- Corinna Lorenz, Xinyu Hao, Tomas Tomka, Linus Rüttimann, and Richard H R Hahnloser. 2022. Interactive extraction of diverse vocal units from a planar embedding without the need for prior sound segmentation. *Front. Bioinform.*, 2:966066.
- Scott Lundberg and Su-In Lee. 2017. A unified approach to interpreting model predictions. *arXiv [cs.AI]*.
- Marius Pachitariu, Nicholas Steinmetz, Shabnam Kadir, Matteo Carandini, and Harris Kenneth D. 2016. Kilosort: realtime spike-sorting for extracellular electrophysiology with hundreds of channels. *bioRxiv*.
- F. Pedregosa, G. Varoquaux, A. Gramfort, V. Michel, B. Thirion, O. Grisel, M. Blondel, P. Prettenhofer, R. Weiss, V. Dubourg, J. Vanderplas, A. Passos, D. Cournapeau, M. Brucher, M. Perrot, and E. Duchesnay. 2011. Scikit-learn: Machine learning in Python. *Journal of Machine Learning Research*, 12:2825–2830.
- Alec Radford, Jeffrey Wu, Rewon Child, David Luan, Dario Amodei, and Ilya Sutskever. 2019. Language models are unsupervised multitask learners.
- Steffen Schneider, Jin Hwa Lee, and Mackenzie Weygandt Mathis. 2023. Learnable latent embeddings for joint behavioural and neural analysis. *Nature*, 617(7960):360–368.
- Jonnathan Singh Alvarado, Jack Goffinet, Valerie Michael, William Liberti, 3rd, Jordan Hatfield, Timothy Gardner, John Pearson, and Richard Mooney. 2021. Neural dynamics underlying birdsong practice and performance. *Nature*, 599(7886):635–639.
- Sindhu Tipirneni and Chandan K Reddy. 2021. Self-supervised transformer for sparse and irregularly sampled multivariate clinical time-series. *arXiv [cs.LG]*.
- Aaron van den Oord, Oriol Vinyals, and Koray Kavukcuoglu. 2017. Neural discrete representation learning. *arXiv [cs.LG]*.
- Ashish Vaswani, Noam Shazeer, Niki Parmar, Jakob Uszkoreit, Llion Jones, Aidan N Gomez, Lukasz Kaiser, and Illia Polosukhin. 2017. Attention is all you need. *arXiv [cs.CL]*.

- 
- Daniel L K Yamins and James J DiCarlo. 2016. Using goal-driven deep learning models to understand sensory cortex. *Nat. Neurosci.*, 19(3):356–365.
- Daniel L K Yamins, Ha Hong, Charles F Cadieu, Ethan A Solomon, Darren Seibert, and James J DiCarlo. 2014. Performance-optimized hierarchical models predict neural responses in higher visual cortex. *Proc. Natl. Acad. Sci. U. S. A.*, 111(23):8619–8624.
- Neil Zeghidour, Alejandro Luebs, Ahmed Omran, Jan Skoglund, and Marco Tagliasacchi. 2021. SoundStream: An end-to-end neural audio codec. *arXiv [cs.SD]*.
- Ding Zhou and Xue-Xin Wei. 2020. Learning identifiable and interpretable latent models of high-dimensional neural activity using pi-VAE. *arXiv [stat.ML]*.

# Appendix A

## Appendix

### A.1 Neuron Depths

Neuron	Depth	Neuron	Depth	Neuron	Depth	Neuron	Depth
N1	3380	N20	2640	N39	2460	N58	2140
N2	3220	N21	2600	N40	2440	N59	2100
N3	3200	N22	2600	N41	2440	N60	1880
N4	3180	N23	2600	N42	2420	N61	1820
N5	2980	N24	2600	N43	2400	N62	1680
N6	2960	N25	2580	N44	2380	N63	1680
N7	2880	N26	2580	N45	2380	N64	1340
N8	2860	N27	2580	N46	2360	N65	1320
N9	2820	N28	2580	N47	2360	N66	1320
N10	2740	N29	2580	N48	2340	N67	1120
N11	2720	N30	2560	N49	2320	N68	1080
N12	2720	N31	2540	N50	2300	N69	1060
N13	2700	N32	2540	N51	2280	N70	1060
N14	2680	N33	2520	N52	2280	N71	840
N15	2680	N34	2520	N53	2260	N72	660
N16	2660	N35	2500	N54	2240	N73	480
N17	2660	N36	2480	N55	2220	N74	480
N18	2640	N37	2480	N56	2180	N75	200
N19	2640	N38	2460	N57	2160		

Table A.1: Depth ( $\mu\text{m}$ ) to probe tip for all neurons used in experiment 1

## A.2 Neural Information Integration

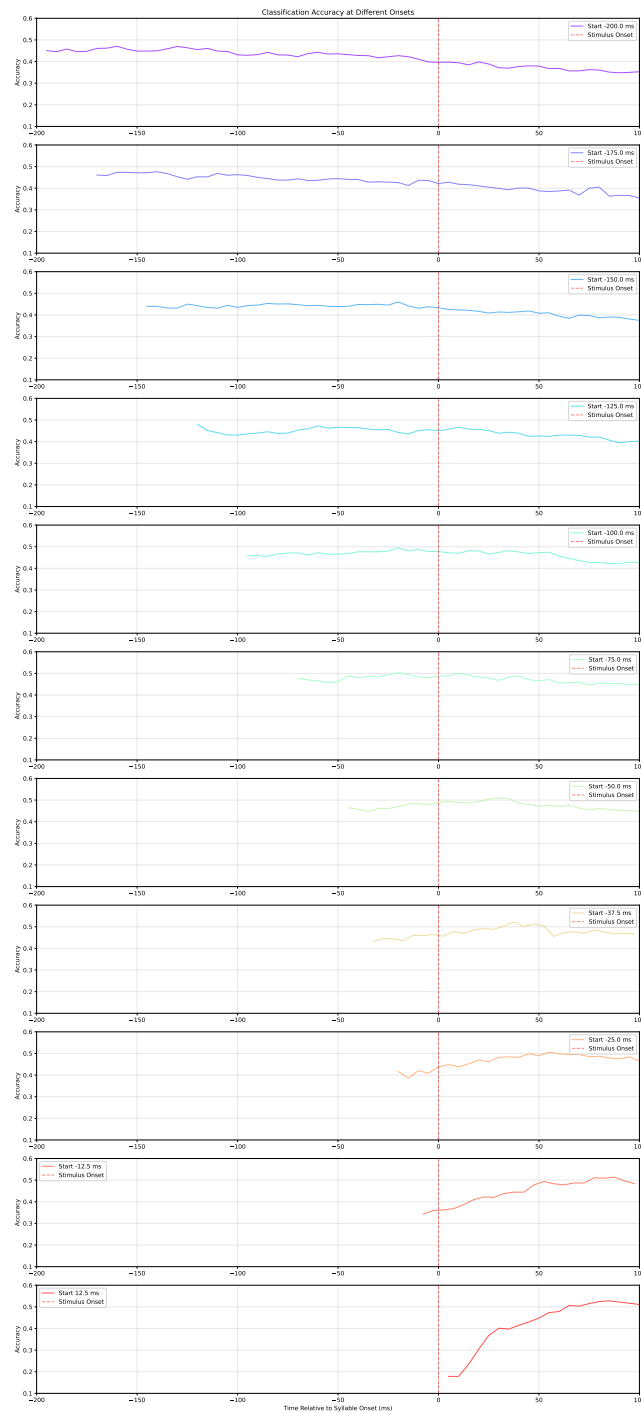


Figure A.1: Classification accuracy at different onsets

### A.3 CEBRA Results

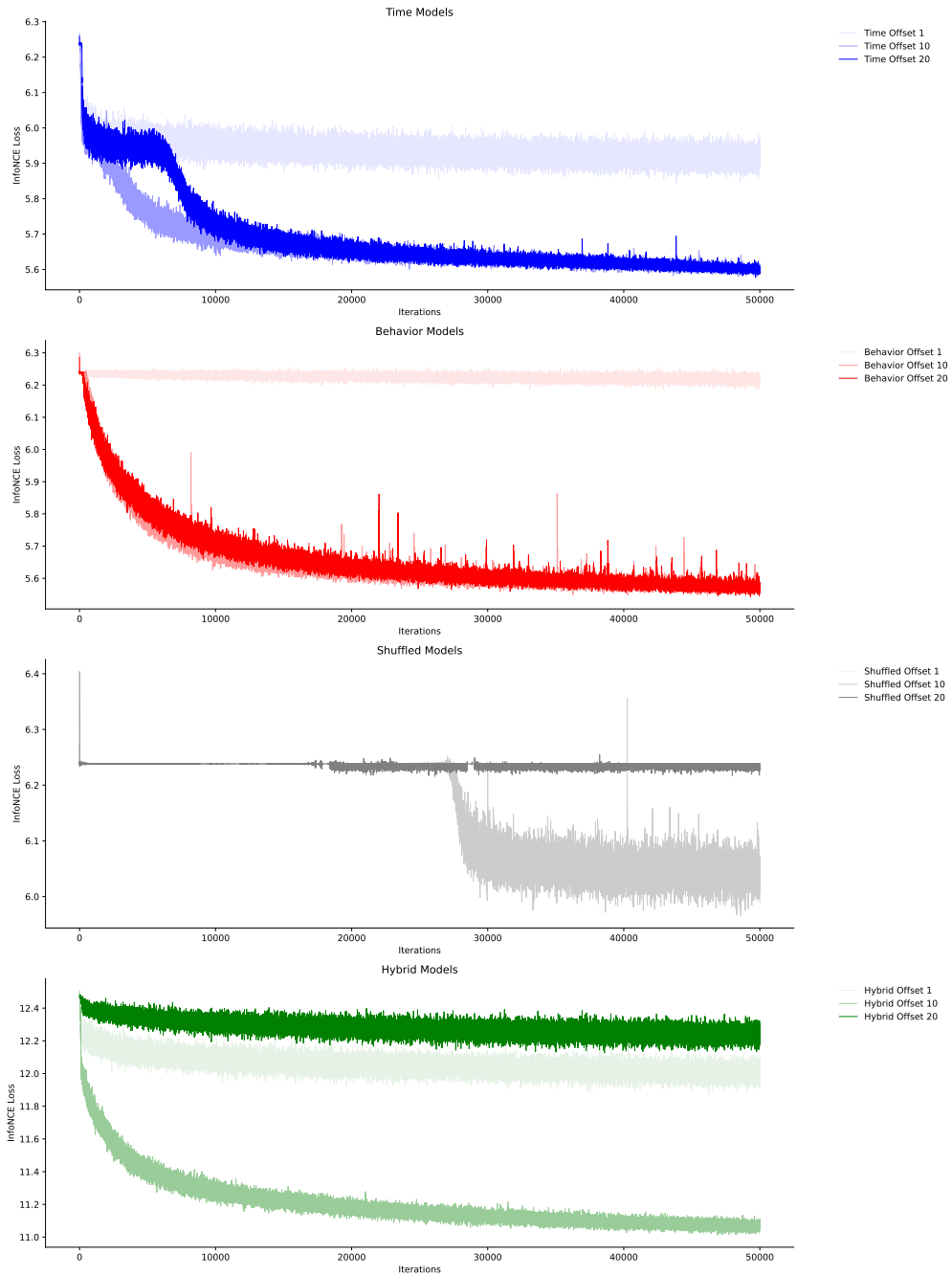


Figure A.3: CEBRA training loss

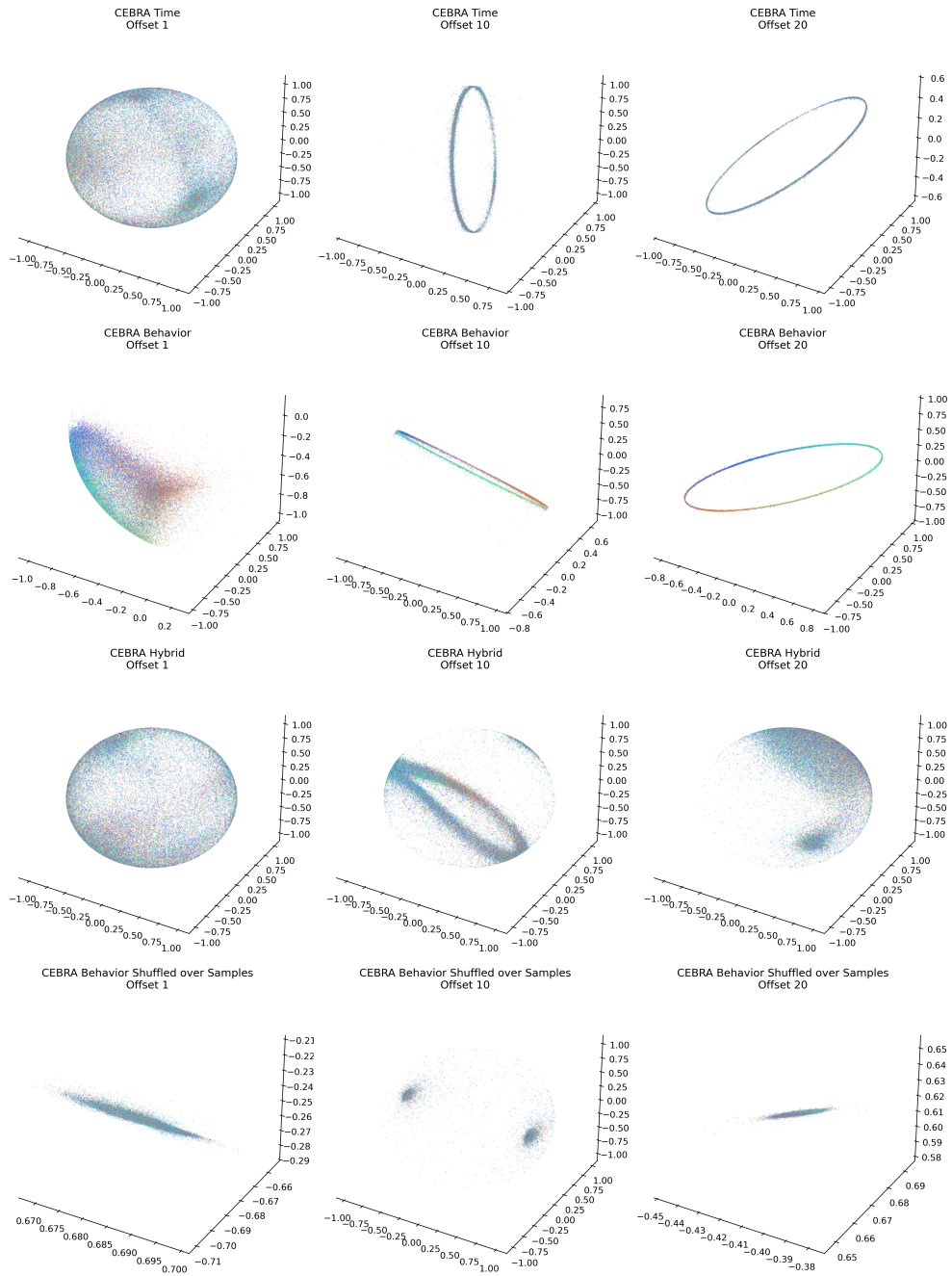


Figure A.2: Extra CEBRA embedding visualization from different parameters

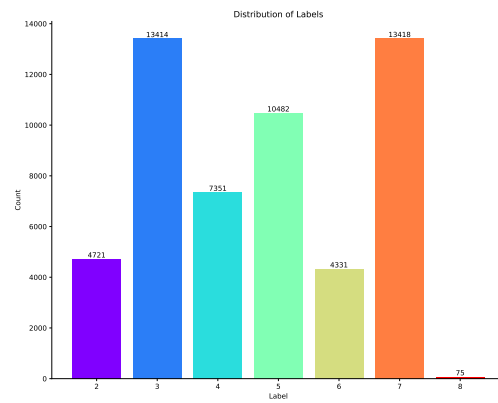
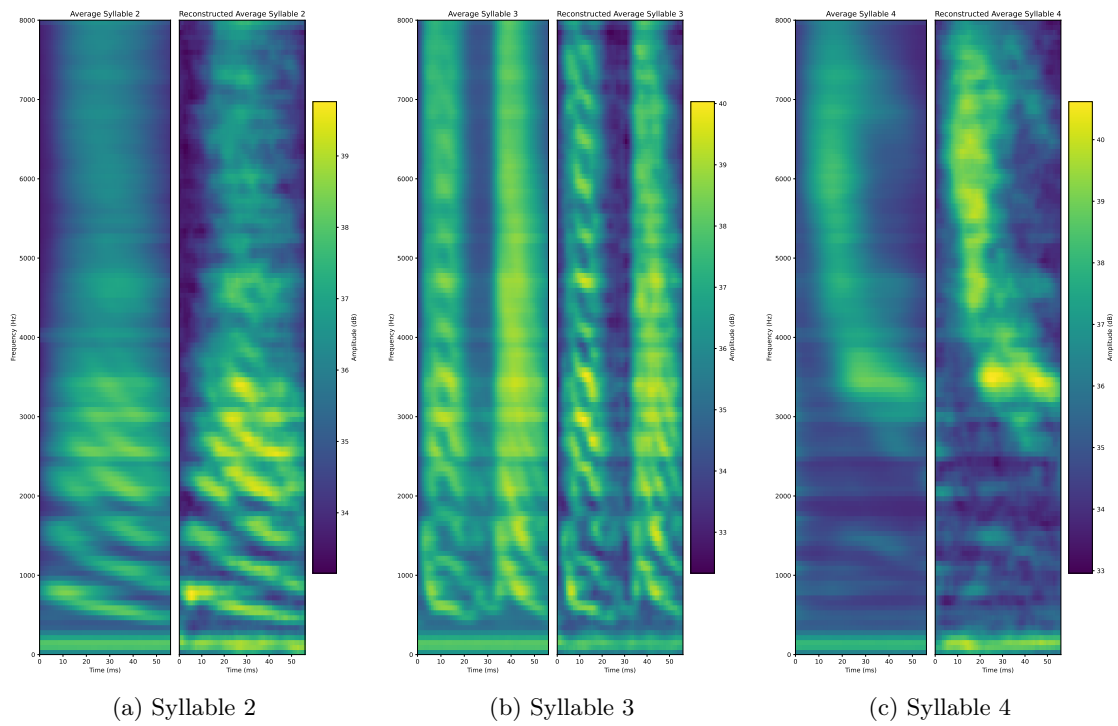


Figure A.4: Data distribution in CEBRA

## A.4 VAE Results



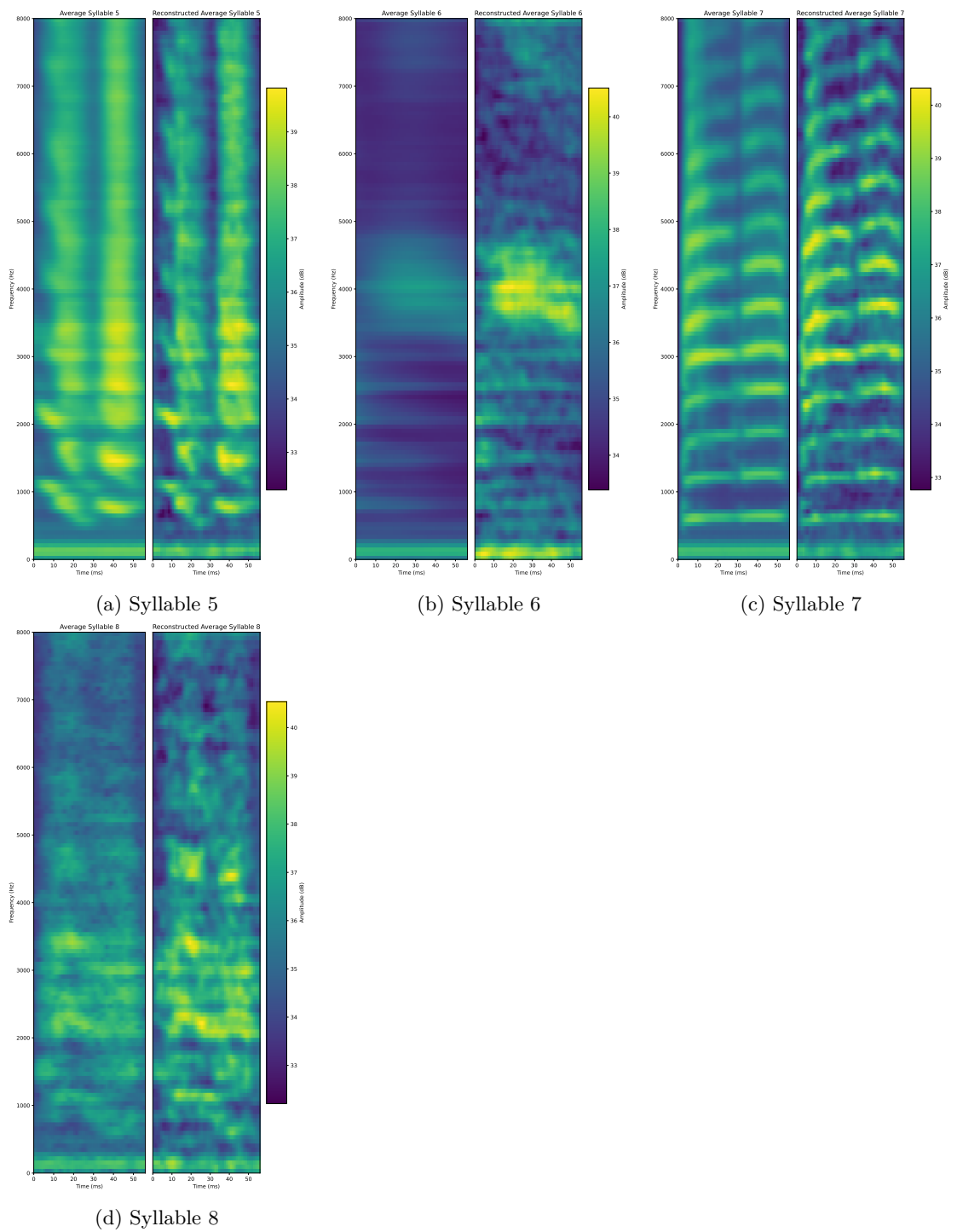


Figure A.6: Original and reconstruction syllables of a motif

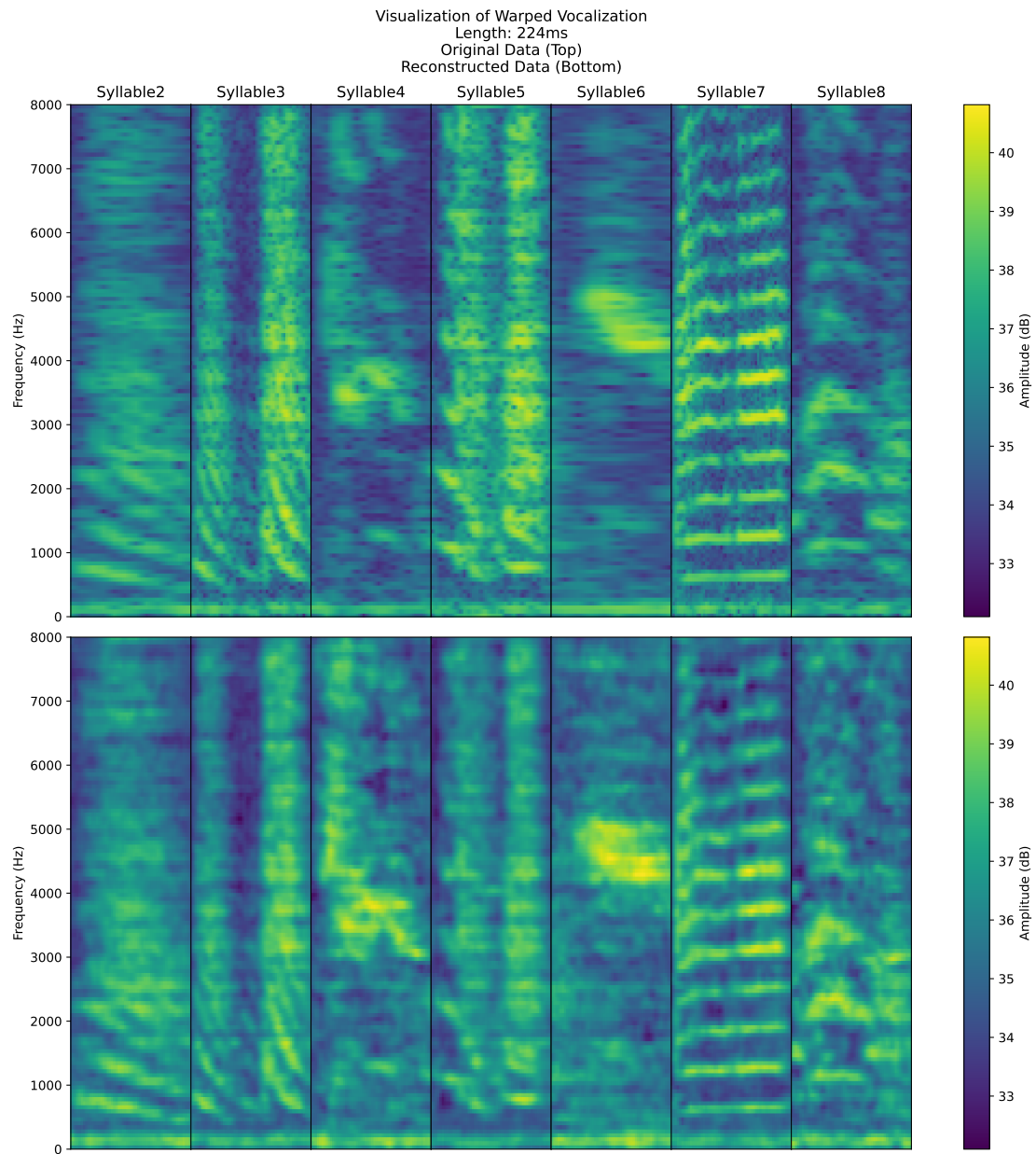


Figure A.7: Reconstruction of warped vocal data

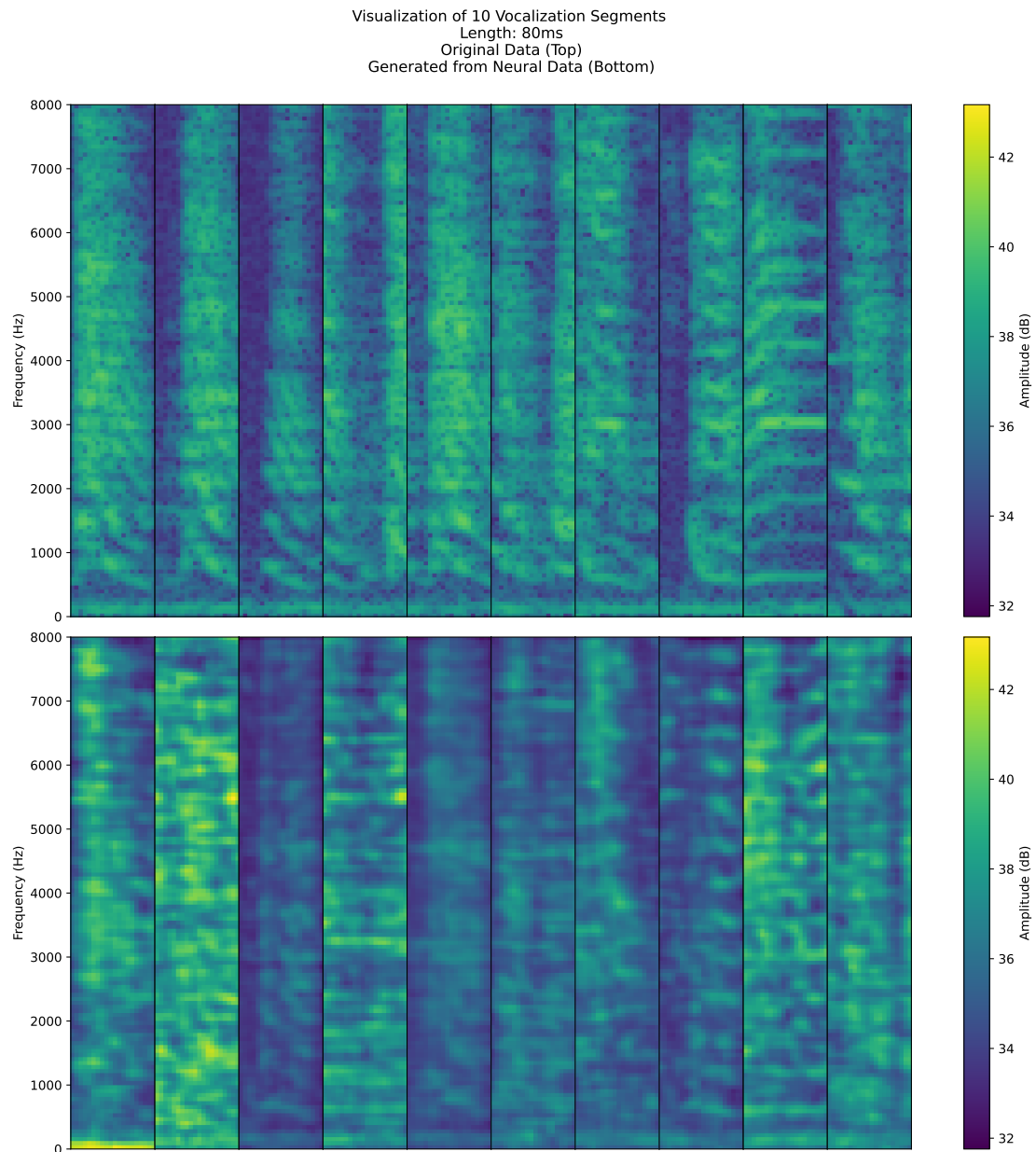


Figure A.8: Generate 80 ms vocalization from 80 ms neural data

# List of Figures

3.1	Quality of clusters . . . . .	9
3.2	Labeled spectrogram for all 7 syllables . . . . .	10
3.3	Distribution of annotated syllables . . . . .	11
4.1	Selective State Space Model . . . . .	12
4.2	Mamba and Mamba-2 structures . . . . .	13
4.3	Transformers architecture . . . . .	16
4.4	VAE architecture . . . . .	19
4.5	VAE reparameterization . . . . .	20
5.1	Classification accuracy using single neuron firing rates . . . . .	24
5.2	Evaluation of total spike counts . . . . .	25
5.3	RF feature importance                      Mean firing rates . . . . .	26
5.4	RF feature importance                      TF-IDF . . . . .	26
5.5	SHAP visualization of neuron importance for classification . . . . .	27
5.6	Neural correlation and interaction analysis . . . . .	29
5.7	Top 10 interactive pairs plotted on a Neuropixels probe . . . . .	30
5.8	Classification accuracy . . . . .	31

5.9	Classification performance in different random time windows . . . . .	32
6.1	Transforming neural data in sampling time into tokens . . . . .	36
6.2	Performance of GPT-2 . . . . .	38
6.3	Mamba confusion matrix with 45 ms sequences . . . . .	38
7.1	Model performance across different window periods . . . . .	43
7.2	Model performance across different bin sizes . . . . .	43
8.1	CEBRA embeddings trained with shuffled behavior labels . . . . .	49
9.1	Reconstruction of binary neural data – 1D VAE . . . . .	58
9.2	Reconstruction of binary neural data – NeuralEnCodec . . . . .	58
9.3	Reconstruction of binned neural data – segments of 40 ms . . . . .	59
9.4	Reconstruction of binned neural data – trimmed to 40 ms . . . . .	59
9.5	Reconstruction of binned neural data – trimmed to 80 ms . . . . .	60
9.6	Reconstruction of binned neural data – padded to 270 ms . . . . .	60
9.7	Reconstruction of segmented vocal data – segments of 40 ms . . . . .	61
9.8	Reconstruction of trimmed vocal data – trimmed to 40 ms . . . . .	62
9.9	Reconstruction of padded vocal data – padded to 224 ms . . . . .	63
9.10	Reconstruction of warped and binned neural data with 1D VAE . . . . .	64
9.11	Reconstruction of binary neural data with NeuralEnCodec . . . . .	64
9.12	Reconstruction of warped vocal data . . . . .	65
9.13	Generate 40 ms vocalization from 40 ms neural data . . . . .	66
9.14	UMAP visualization of latent representations from generation experiment	67
9.15	UMAP visualization of latent representations from neuro2voc experiment	67

---

9.16 UMAP visualization of latent representations from correlation experiment	68
9.17 Result from canonical component analysis . . . . .	69
A.1 Classification accuracy at different onsets . . . . .	82
A.3 CEBRA training loss . . . . .	83
A.2 Extra CEBRA embedding visualization from different parameters . . . . .	84
A.4 Data distribution in CEBRA . . . . .	85
A.6 Original and reconstruction syllables of a motif . . . . .	86
A.7 Reconstruction of warped vocal data . . . . .	87
A.8 Generate 80 ms vocalization from 80 ms neural data . . . . .	88

# List of Tables

3.1	Duration of recordings across different sessions . . . . .	8
5.1	Classification accuracy . . . . .	23
6.1	GPT-2 classification accuracy with sequences from 15 ms to 60 ms . . . . .	37
7.1	Top-3 parameter combinations for each model on accuracy . . . . .	42
7.2	Model performance on sampling time . . . . .	44
8.2	Model performance comparison on sequences . . . . .	50
8.1	Model performance across different CEBRA parameters . . . . .	51
9.1	Syllable classification accuracies (%) . . . . .	69
A.1	Depth ( $\mu\text{m}$ ) to probe tip for all neurons used in experiment 1 . . . . .	81

# List of Acronyms

AFP	anterior forebrain pathway
area X	area X of the paraolfactory lobe
CCA	Canonical Correlation Analysis
CNN	Convolutional Neural Network
CVE	Continuous Value Embedding
DLM	dorsolateral division of the medial thalamus
EEG	Electroencephalogram
HVC	Hyperstriatum Ventralis pars caudalis
KLD	Kullback-Leibler Divergence
LMAN	Lateral nucleus Magnocellularis of the Anterior Neostriatum
LSTM	Long Short-Term Memory
MEG	Magnetoencephalogram
MSE	Mean Squared Error
NLP	Natural Language Processing
RA	Nucleus Robustus of the Archistriatum
RBF	Radial Basis Function
RF	Random Forest
SVM	Support Vector Machine
SSM	State-Space Model
t-SNE	t-distributed Stochastic Neighbor Embedding
UMAP	Uniform Manifold Approximation and Projection
VAE	Variational Auto Encoder